Commun. Comput. Phys.
doi: 10.4208/cicp.210709.210610a

Vol. **10**, No. 1, pp. 1-31
July 2011

All Speed Scheme for the Low Mach Number Limit of the Isentropic Euler Equations

Pierre Degond and Min Tang*

Institute of Mathematics of Toulouse, Université Paul Sabatier, 118, route de Narbonne, 31062 Toulouse cedex, France.

Received 21 July 2009; Accepted (in revised version) 21 June 2010

Available online 7 February 2011

Abstract. An all speed scheme for the Isentropic Euler equations is presented in this paper. When the Mach number tends to zero, the compressible Euler equations converge to their incompressible counterpart, in which the density becomes a constant. Increasing approximation errors and severe stability constraints are the main difficulty in the low Mach regime. The key idea of our all speed scheme is the special semi-implicit time discretization, in which the low Mach number stiff term is divided into two parts, one being treated explicitly and the other one implicitly. Moreover, the flux of the density equation is also treated implicitly and an elliptic type equation is derived to obtain the density. In this way, the correct limit can be captured without requesting the mesh size and time step to be smaller than the Mach number. Compared with previous semi-implicit methods [11,13,29], firstly, nonphysical oscillations can be suppressed by choosing proper parameter, besides, only a linear elliptic equation needs to be solved implicitly which reduces much computational cost. We develop this semi-implicit time discretization in the framework of a first order Local Lax-Friedrichs (or Rusanov) scheme and numerical tests are displayed to demonstrate its performances.

AMS subject classifications: 65M06, 65Z05, 76N99, 76L05

Key words: Low Mach number, Isentropic Euler equations, compressible flow, incompressible limit, asymptotic preserving, Rusanov scheme.

1 Introduction

Singular limit problems in fluid mechanics have drawn great attentions in the past years, like low-Mach number flows, magneto-hydrodynamics at small Mach and Alfven numbers and multiple-scale atmospheric flows. As mentioned in [17], the singular limit regime induces severe stiffness and stability problems for standard computational techniques. In this paper, we focus on the simplest Isentropic Euler equations and propose a

*Corresponding author. *Email addresses:* degond@mip.ups-tlse.fr (P. Degond), tangmin1002@gmail.com (M. Tang)

numerical scheme that is uniformly applicable and efficient for all ranges of Mach numbers.

The problem under study is the Isentropic Euler equations

$$\begin{cases} \partial_t \rho_\epsilon + \nabla \cdot (\rho_\epsilon \mathbf{u}_\epsilon) = 0, \\ \partial_t (\rho_\epsilon \mathbf{u}_\epsilon) + \nabla (\rho_\epsilon \mathbf{u}_\epsilon \otimes \mathbf{u}_\epsilon) + \dfrac{1}{\epsilon^2} \nabla p_\epsilon = 0, \end{cases} \tag{1.1}$$

where $\rho_\epsilon, \rho_\epsilon \mathbf{u}_\epsilon$ is the density and momentum of the fluid respectively and ϵ is the scaled Mach number. This is one of the most studied nonlinear hyperbolic systems. For standard applications, the equation of state takes the form

$$p(\rho) = \Lambda \rho^\gamma, \tag{1.2}$$

where Λ, γ are constants depending on the physical problem.

It is rigorously proved by Klainerman and Majda [15,16] that when $\epsilon \to 0$, i.e., when the fluid velocity is small compared with the speed of sound [3], the solution of (1.1) converges to its incompressible counterpart. Formally, this can be obtained by inserting the expansion

$$\rho_\epsilon = \rho_0 + \epsilon^2 \rho_{(2)} + \cdots, \tag{1.3a}$$

$$\mathbf{u}_\epsilon = \mathbf{u}_0 + \epsilon^2 \mathbf{u}_{(2)} + \cdots, \tag{1.3b}$$

into (1.1) and equate the same order of ϵ. The limit reads as follows [15,18]:

$$\rho = \rho_0, \tag{1.4a}$$

$$\nabla \cdot \mathbf{u}_0 = 0, \tag{1.4b}$$

$$\partial_t \mathbf{u}_0 + \nabla (\mathbf{u}_0 \otimes \mathbf{u}_0) + \nabla p_{(2)} = 0. \tag{1.4c}$$

Here $p_{(2)}$ is a scalar pressure which can be viewed as the Lagrange multiplier of the incompressibility constraint. In view of the discussion of [17,18], p_0 is the thermodynamic pressure, which is uniform in the low Mach number limit, and $p_{(2)}$ is the hydrodynamic pressure. Low Mach number flows are flows which are slow compared with the speed of sound. In such a situation, pressure waves become very fast and, in the zero Mach number limit, an instantaneous pressure equalization takes place [24,25].

For atmosphere-ocean computing or fluid flows in engineering devices, when ϵ is small in (1.1), standard numerical methods become unacceptably expensive. Indeed, (1.1) has wave speeds of the form

$$\lambda = \mathbf{u}_\epsilon \pm \frac{1}{\epsilon} \sqrt{p'(\rho_\epsilon)},$$

where $p'(\rho_\epsilon)$ is the derivative with respect to ρ_ϵ. If a standard hyperbolic solver is used, the CFL requirement is $\Delta t = \mathcal{O}(\epsilon \Delta x)$. Moreover in order to maintain stability, the numerical dissipation required by the hyperbolic solver is proportional to $|\lambda|$. If $|\lambda| = \mathcal{O}(1/\epsilon)$,

in order to control the diffusion, we need to have $\Delta x = o(\epsilon^r)$, where r is some appropriate constant. Thus the stability and accuracy highly depend on ϵ.

Our aim is to design a method whose stability and accuracy is independent of ϵ and which will be applicable for Mach numbers ranging from very small to order one values. Such a method is referred to as an "all-speed scheme". The design of an all-speed scheme is primarily a mathematical and numerical issue. Indeed, on the one-hand, the scheme must capture the shocks which can develop in the finite Mach number case but, on the other hand, it has to be uniformly stable and accurate when the Mach number tends to zero i.e., close to the incompressible regime. These are two somehow antagonist demands which are hard to fulfil simultaneously. The goal of this paper is to present and validate the basic concepts of a scheme having such features in a simplified framework. To this aim, it is preferable to use a simplified model which carries all the mathematical difficulties, even at the price of a less physically realistic description. We will use the isentropic Euler model which exhibits both finite and small Mach number regimes and is a perfect laboratory for this problem. Of course, the physical relevance of the isentropic model for large number flows can be questioned. In a future work, we will demonstrate that the present numerical strategies stay valid in the more physically realistic case of the full Euler model.

The idea is to find an asymptotic preserving (AP) method, i.e., a method which gives a consistent discretization of the Isentropic Euler equations (1.1), when $\Delta x, \Delta t$ resolve ϵ, and a consistent discretization of the incompressible limit (1.4), when $\epsilon \to 0$ ($\Delta x, \Delta t$ being fixed). The efficiency of AP schemes at the low Mach number regime can be proved similarly as in [9]. The key idea of our all speed scheme is a specific semi-implicit time discretization, in which the low Mach number stiff term is divided into two parts, one part being treated explicitly and the other one implicitly. Moreover, the flux of the density equation is also treated implicitly. For the space discretization, when ϵ is $\mathcal{O}(1)$, even if the initial condition is smooth, shocks will form due to the nonlinearity of the $\mathrm{div}\left(\rho_\epsilon \mathbf{u}_\epsilon \otimes \mathbf{u}_\epsilon\right)$ term and shock capturing methods should be employed here.

In the literature, lots of efforts have been made to find numerical schemes for the compressible equations that can also capture the zero Mach number limit [1, 6, 11, 24, 25]. In [1], Bijl and Wesseling split the pressure into thermodynamic and hydrodynamic pressure terms and solve them separately. Similar to this approach, the multiple pressure variable (MPV) method was proposed by Munz et al. in [24,25]. There is also some recent work by Hauck et al. [11]. Their approach involves specific splitting of the pressure term. We avoid using this splitting, the proper design of which seems very crucial in some cases.

Similar ideas can be found in the Implicit Continuous-Fluid Eulerian (ICE) method, which is designed to adapt incompressible flow computation techniques using staggered meshes to the simulation compressible flows. The method was first introduced by Harlow and Amsdan in 1965 and 1971 [12,13]. It has been used to simulate single phase fluid dynamic problems with all flow speeds. They introduce two parameters in the continuity equation and the momentum equation to combine information from both previous and

forward time steps. However this method is not conservative, which leads to discrepancies in the shock speeds. Additionally it suffers from small wiggles when there are moving contact discontinuities. The first problem was solved by an iterative method, for example SIMPLE [26], or PISO [14]. In some recent work, Heul and Wesseling also find a conservative pressure-correction method [29]. All these methods are based on the so called MAC staggered mesh in order to be consistent with the staggered grid difference method for the incompressible Euler equations [13]. Specifically, if we write the simplified ICE technique presented in [2] in conservative form, we are led to the semi-discrete framework:

$$\begin{cases} \dfrac{\rho_\epsilon^*-\rho_\epsilon^n}{\Delta t}+\nabla\cdot(\rho_\epsilon\mathbf{u}_\epsilon)^n=0, \\ \dfrac{(\rho_\epsilon\mathbf{u}_\epsilon)^*-(\rho_\epsilon\mathbf{u}_\epsilon)^n}{\Delta t}+\nabla(\rho_\epsilon^n\mathbf{u}_\epsilon^n\otimes\mathbf{u}_\epsilon^n)=0, \end{cases} \tag{1.5a}$$

$$\begin{cases} \dfrac{\rho_\epsilon^{n+1}-\rho_\epsilon^*}{\Delta t}+\nabla\cdot\big((\rho_\epsilon\mathbf{u}_\epsilon)^{n+1}-(\rho_\epsilon\mathbf{u}_\epsilon)^*\big)=0, \\ \dfrac{(\rho_\epsilon\mathbf{u}_\epsilon)^{n+1}-(\rho_\epsilon\mathbf{u}_\epsilon)^*}{\Delta t}+\dfrac{1}{\epsilon^2}\nabla p(\rho_\epsilon^{n+1})=0. \end{cases} \tag{1.5b}$$

By substituting the gradient of the second equation of (1.5b) into its first equation and using the results of the first equation (1.5a), ρ_ϵ can be updated by solving an elliptic equation which does not degenerate when $\epsilon\to 0$.

We use a similar idea in our method. However, we do not use the predictor-corrector procedure but we rather discretize the problem in a single step. We use standard shock capturing schemes which guarantee the conservativity and the desired artificial viscosity. We only use implicit evaluations of the mass flux and pressure gradient terms to ensure stability and we provide an extremely simple way to deal with the implicitness. Additionally, we propose a modification of the implicit treatment of the pressure equation. Indeed, using a similar idea as in [11], we split the pressure into two parts and put $\alpha p(\rho_\epsilon)$ into the hyperbolic system, where α is a suitable parameter between 0 and $1/\epsilon^2$. This makes the first system strictly hyperbolic and therefore, much more stable (if $\alpha=0$ the hyperbolic system is only weakly hyperbolic and develops weak instabilities which grow like a power of the time). The choice of this parameter α depends on the time and space steps and on the specific problem. As long as the solution does not involve any shock (be it in the low or finite Mach number regimes), α can be chosen equal to 0. However, when dealing with strong shocks, α must be increased. Ideally, the choice of α should be made dependent on space and time. In the present paper, in order to provide a reliable assessment of the role of α, it is kept constant in space but can depend on time. The investigation of strategies which would allow α to depend on both space and time is deferred to future work.

The numerical results show the advantage of our method in the following sense:

- The method is in conservative form and can capture the right shock speeds.

• Compared with previous semi-implicit methods [11, 13, 29], only a linear elliptic equation needs to be solved implicitly which reduces much computational cost.

• The non-physical oscillations [10] can be suppressed by choosing the proper value of the parameter which determines the fraction of implicitness used in the evaluation of the pressure gradient term.

In this paper we only use the first order Local Lax-Friedrichs (or Rusanov) scheme [22, 28]. Higher order space and time discretizations will be subject of future work. The main objective of this work is to show that the semi-discrete time discretization provides a framework for developing AP methods for singular limit problems. Similar ideas can be extended to the full Euler equations and more complicated fluid model and have also been used in other contexts such as quasi neutrality limits [4, 7] and magnetized fluids under strong magnetic fields [5].

The organization of this paper is as follows. Section 2 exposes the semi-implicit scheme and its capability to capture the incompressible limit is proved. The detailed one dimensional and two dimensional fully discretized schemes and their AP property are presented in Sections 3 and 4 respectively. In Section 5, how to choose the ad-hoc parameter is discussed and finally, some numerical tests are given in Section 6 to discuss the stability and accuracy of our scheme. The efficiency at both the compressible and low Mach number regime are displayed. Finally, we conclude in Section 6 with some discussion.

2 Time semi-discrete scheme

Let Δt be the time step,

$$t^n = n\Delta t, \quad n = 0,1,\cdots,$$

and let the "n" superscript denote the approximations at t^n. The semi-discrete scheme for the nth time step is

$$\frac{\rho_\epsilon^{n+1}-\rho_\epsilon^n}{\Delta t} + \nabla\cdot(\rho_\epsilon \mathbf{u}_\epsilon)^{n+1} = 0, \tag{2.1a}$$

$$\frac{(\rho_\epsilon \mathbf{u}_\epsilon)^{n+1}-(\rho_\epsilon \mathbf{u}_\epsilon)^n}{\Delta t} + \mathrm{div}\left(\rho_\epsilon^n \mathbf{u}_\epsilon^n \otimes \mathbf{u}_\epsilon^n + \alpha p(\rho_\epsilon^n)\right) + \frac{1-\alpha\epsilon^2}{\epsilon^2}\nabla p(\rho_\epsilon^{n+1}) = 0, \tag{2.1b}$$

where α is an ad-hoc parameter, which satisfies $\alpha \le 1/\epsilon^2$. The choice of α depends on the space and time steps and on the fluid speed. When the shock is strong, α should be bigger, which means that the system should be more explicit to follow the discontinuity more closely. We discuss the choice of α for specific equations of state in this paper and test its effect numerically. It depends on the required accuracy, the small parameter ϵ and the shock amplitude in a sometimes quite complex way.

Rewriting the momentum equation (2.1b) as

$$(\rho_\epsilon \mathbf{u}_\epsilon)^{n+1} = (\rho_\epsilon \mathbf{u}_\epsilon)^n - \Delta t\nabla\left(\rho_\epsilon^n \mathbf{u}_\epsilon^n \otimes \mathbf{u}_\epsilon^n + \alpha p(\rho_\epsilon^n)\right) - \Delta t\frac{1-\alpha\epsilon^2}{\epsilon^2}\nabla p(\rho_\epsilon^{n+1})$$

and substituting it into the density equation, one gets

$$\rho_\epsilon^{n+1}-\Delta t^2\frac{1-\alpha\epsilon^2}{\epsilon^2}\Delta p(\rho_\epsilon^{n+1})=\phi(\rho_\epsilon^n,\mathbf{u}_\epsilon^n), \tag{2.2}$$

which is an elliptic equation that can be solved relatively easily. Here

$$\phi(\rho_\epsilon^n,\mathbf{u}_\epsilon^n)=\rho_\epsilon^n-\Delta t\nabla\cdot(\rho_\epsilon^n\mathbf{u}_\epsilon^n)+\Delta t^2\nabla\cdot\nabla\big(\rho_\epsilon^n\mathbf{u}_\epsilon^n\otimes\mathbf{u}_\epsilon^n+\alpha p(\rho_\epsilon^n)\big). \tag{2.3}$$

The Laplace operator in (2.2) can be approximated by $\nabla\big(p'(\rho_\epsilon^n)\nabla\rho_\epsilon^{n+1}\big)$ and (2.2) becomes

$$\rho_\epsilon^{n+1}-\Delta t^2\frac{1-\alpha\epsilon^2}{\epsilon^2}\nabla\cdot\big(p'(\rho_\epsilon^n)\nabla\rho_\epsilon^{n+1}\big)=\phi(\rho_\epsilon^n,\mathbf{u}_\epsilon^n). \tag{2.4}$$

The diffusion term

$$\Delta t^2\frac{1-\alpha\epsilon^2}{\epsilon^2}\nabla\cdot\big(p'(\rho_\epsilon^n)\nabla\rho_\epsilon^{n+1}\big)$$

plays the role of a numerical viscosity term (see Section 5), when $\Delta t/\epsilon^2\ll 1$, this additional diffusion is of the same order as that introduced by standard shock capturing schemes. However, when $\Delta t/\epsilon^2\gg 1$, this term contributes to relax the solution towards the incompressible limit.

When we implement this method, ρ_ϵ^{n+1} can be obtained from (2.2) first and $\mathbf{u}_\epsilon^{n+1}$ is then computed using the momentum equation (2.1b) afterwards. Therefore, apart from the resolution of the elliptic equation (2.4), the scheme only involves explicit steps.

We now show that the scheme (2.1a) and (2.1b) is asymptotic preserving. We introduce the formal expansion

$$\rho_\epsilon^n(x)=\rho_{(0)c}^n+\epsilon\rho_{(1)}^n(x)+\epsilon^2\rho_{(2)}^n(x)+\cdots, \tag{2.5a}$$

$$\mathbf{u}_\epsilon^n=\mathbf{u}_{(0)}^n(x)+\epsilon\mathbf{u}_{(1)}^n(x)+\cdots. \tag{2.5b}$$

In the sequel, the "c" in the index means that the quantity is independent of space. When Δx, Δt are fixed and ϵ goes to 0 in (2.2), we formally have $\Delta p(\rho_0^{n+1})=0$, which implies that ρ_0^{n+1} is independent of space, where ρ_0^{n+1} is the limit of ρ_ϵ^{n+1} when $\epsilon\to 0$. Thus we have

$$\frac{\rho_{(0)c}^{n+1}-\rho_{(0)c}^n}{\Delta t}+\nabla\cdot\big(\rho_{(0)c}\mathbf{u}_{(0)}\big)^{n+1}=0 \tag{2.6}$$

by equating the $\mathcal{O}(1)$ terms in the density equation (2.1a). Integrating (2.6) over the computational domain, one gets

$$|\Omega|\frac{\rho_{(0)c}^{n+1}-\rho_{(0)c}^n}{\Delta t}=-\rho_{(0)c}^{n+1}\int_\Omega\nabla\cdot\big(\mathbf{u}_{(0)}\big)^{n+1}=-\rho_{(0)c}^{n+1}\int_{\partial\Omega}\mathbf{n}\cdot\mathbf{u}_{(0)}^{n+1}. \tag{2.7}$$

As discussed in [11], for wall boundary condition, periodic boundary condition and open boundary condition, (2.7) gives

$$\rho_{(0)c}^{n+1}=\rho_{(0)c}^n, \tag{2.8}$$

that is ρ_0 is also independent of time. Thus (2.6) also implies

$$\nabla\cdot\mathbf{u}_{(0)}^{n+1}=0. \tag{2.9}$$

Then, by using the fact that the curl of the gradient of any scalar field is always zero, the curl of the $\mathcal{O}(1)$ terms of the momentum equation (2.1b) becomes

$$\nabla\times\frac{\mathbf{u}_{(0)}^{n+1}-\mathbf{u}_{(0)}^{n}}{\Delta t}+\nabla\times\nabla\left(\mathbf{u}_{(0)}^{n}\otimes\mathbf{u}_{(0)}^{n}\right)=0. \tag{2.10}$$

Thus

$$\frac{\mathbf{u}_{(0)}^{n+1}-\mathbf{u}_{(0)}^{n}}{\Delta t}+\nabla\left(\mathbf{u}_{(0)}^{n}\otimes\mathbf{u}_{(0)}^{n}\right)+\nabla p_{(2)}^{n}=0, \tag{2.11}$$

where $p_{(2)}^{n}$ is some scalar field.

Eqs. (2.8), (2.9) and (2.11) are the semi-discretization in time of (1.4) and thus the scheme (2.1a) and (2.1b) is consistent with the low Mach number limit $\epsilon\to 0$ of the original compressible Euler equations. This statement is exactly saying that the scheme is AP. We can see that, in order to obtain the stability and AP properties, it is crucial to treat the flux in the density equation (2.1a) implicitly.

Letting $U=(\rho_\epsilon,\rho_\epsilon\mathbf{u}_\epsilon)^T$, we can write (2.1a), (2.1b) abstractly as

$$\frac{U^{n+1}-U^{n}}{\Delta t}+\nabla\cdot F\left(U^{n+\frac{1}{2}}\right)+QU^{n+1}=0, \tag{2.12}$$

where

$$F(U^{n+\frac{1}{2}})=\begin{pmatrix}(\rho_\epsilon\mathbf{u}_\epsilon)^{n+1}\\ \rho_\epsilon^{n}\mathbf{u}_\epsilon^{n}\otimes\mathbf{u}_\epsilon^{n}+\alpha p(\rho_\epsilon^{n})\end{pmatrix},\qquad Q=\begin{pmatrix}0 & 0\\ \frac{1-\alpha\epsilon^2}{\epsilon^2}\nabla p(\rho_\epsilon^{n+1}) & 0\end{pmatrix}. \tag{2.13}$$

Here p is an operator on ρ_ϵ and $U^{n+1/2}$ reminds that the flux is partly implicit and partly explicit.

This semi-discretization gives us a framework for developing AP schemes that can capture the incompressible limit. Now we are left with the problem of how discretizing the space variable. Because shocks can form, considerable literature has been devoted to the design of high resolution methods that can capture the correct shock speed. Upwind schemes and central schemes are among the most widely used Godunov type schemes [19–21].

In the following section, we propose a space discretization of the second term of (2.12) using an upwind solver, while that of the third term of (2.12) uses a central scheme. The implicitness of the density flux is treated by combining it with the momentum equation which results in a discrete elliptic equation for the density ρ^{n+1}. In the present work, for the sake of simplicity, we only consider an upwind scheme based on the first order Rusanov scheme with local evaluation of the wave-speed in the current and neighboring cell.

3 Full time and space discretization: one dimensional case

For simplicity, we consider the domain $\Omega=[0,1]$. Using a uniform spatial mesh with $\Delta x=1/M$, M being an positive integer, the grid points are defined as $x_j=j\Delta x$, $j=0,1,\cdots,M$, and $U=(\rho_\epsilon,\rho_\epsilon u_\epsilon)$, where $\mathbf{u}_\epsilon$ now becomes a scalar and we use u_ϵ to denote the velocity in one dimension.

The flux and Jacobian matrix of (2.12) become

$$F(U)=\begin{pmatrix}\rho_\epsilon u_\epsilon\\ \rho_\epsilon u_\epsilon^2+\alpha p(\rho_\epsilon)\end{pmatrix},\qquad F'(U)=\begin{pmatrix}0 & 1\\ -u_\epsilon^2+\alpha p'(\rho_\epsilon) & 2u_\epsilon\end{pmatrix},\tag{3.1}$$

so, the wave speeds are

$$\lambda=u_\epsilon\pm\sqrt{\alpha p'(\rho_\epsilon)}.\tag{3.2}$$

Let U_j be the approximation of $U(x_j)$ and let

$$A_{j+\frac{1}{2}}(t)=\max\{|\lambda_j|,|\lambda_{j+1}|\}.\tag{3.3}$$

These are the local maximal wave-speeds in the current and neighboring cells. We discretize (2.12) in space as follows:

$$\frac{U_j^{n+1}-U_j^n}{\Delta t}+D_j^xF\big(U^{n+\frac{1}{2}}\big)+\frac{1}{2}\Big(A_{j-\frac{1}{2}}D_{j-}^x-A_{j+\frac{1}{2}}D_{j+}^x\Big)U^n+Q_jU^{n+1}=0,\tag{3.4}$$

where

$$D_j^xu=\frac{u_{j+1}-u_{j-1}}{2\Delta x},\qquad D_{j+}^xu=\frac{u_{j+1}-u_j}{\Delta x},\qquad D_{j-}^xu=\frac{u_j-u_{j-1}}{\Delta x},\tag{3.5a}$$

$$F_j(U^{n+\frac{1}{2}})=\begin{pmatrix}(\rho_\epsilon u_\epsilon)_j^{n+1}\\ (\rho_\epsilon u_\epsilon^2)_j^n+\alpha p(\rho_{\epsilon j}^n)\end{pmatrix},\qquad Q_jU^{n+1}=\begin{pmatrix}0\\ \frac{1-\alpha\epsilon^2}{\epsilon^2}D_j^xp(\rho_\epsilon^{n+1})\end{pmatrix}.\tag{3.5b}$$

Let

$$q_\epsilon=\rho_\epsilon u_\epsilon,\tag{3.6a}$$

$$F_{\rho_\epsilon j}^n=D_j^xq_\epsilon^n+\frac{1}{2}\Big(A_{j-\frac{1}{2}}D_{j-}^x-A_{j+\frac{1}{2}}D_{j+}^x\Big)\rho_\epsilon^n,\tag{3.6b}$$

$$F_{q_\epsilon j}^n=D_j^x\Big(\frac{q_\epsilon^{n2}}{\rho_\epsilon^n}+\alpha p(\rho_\epsilon^n)\Big)+\frac{1}{2}\Big(A_{j-\frac{1}{2}}D_{j-}^x-A_{j+\frac{1}{2}}D_{j+}^x\Big)q_\epsilon^n.\tag{3.6c}$$

We can rewrite the momentum discretization in (3.4) as follows:

$$q_{\epsilon j}^{n+1}=q_{\epsilon j}^n-\Delta tF_{q_\epsilon j}^n-\Delta t\frac{1-\alpha\epsilon^2}{\epsilon^2}D_j^xp(\rho_\epsilon^{n+1}).\tag{3.7}$$

By substituting (3.7) into the density equation in (3.4), one gets

$$\rho_{\epsilon j}^{n+1}-\frac{(1-\alpha\epsilon^2)\Delta t^2}{4\epsilon^2\Delta x^2}\Big(p\big(\rho_{\epsilon j+2}^{n+1}\big)-2p\big(\rho_{\epsilon j}^{n+1}\big)+p\big(\rho_{\epsilon j-2}^{n+1}\big)\Big)=D\phi(\rho_\epsilon^n,q_\epsilon^n), \tag{3.8}$$

where

$$D\phi(\rho_\epsilon^n,q_\epsilon^n)=\rho_\epsilon^n-\Delta tF_{\rho_\epsilon j}^n+\Delta t^2D_j^xF_{q_\epsilon}^n \tag{3.9}$$

is a discretization of $\phi(\rho_\epsilon^n,u_\epsilon^n)$ in (2.3). We notice that (3.8) is a discretization of the elliptic equation (2.4). We can update q_ϵ^{n+1} through (3.7) afterwards.

To obtain ρ_ϵ^{n+1} in (3.8), a nonlinear system of equations needs to be solved. One possible way to simplify it is to replace $\nabla p(\rho_\epsilon^{n+1})$ by $p'(\rho_\epsilon^n)\nabla\rho_\epsilon^{n+1}$, so that the following linear system is obtained:

$$\rho_{\epsilon j}^{n+1}-\frac{(1-\alpha\epsilon^2)\Delta t^2}{4\epsilon^2\Delta x^2}\Big(p'(\rho_{\epsilon j+1}^n)\big(\rho_{\epsilon j+2}^{n+1}-\rho_{\epsilon j}^{n+1}\big)-p'(\rho_{\epsilon j-1}^n)\big(\rho_{\epsilon j}^{n+1}-\rho_{\epsilon j-2}^{n+1}\big)\Big)=D\phi(\rho_\epsilon^n,q_\epsilon^n). \tag{3.10}$$

This is a five point scheme which is too much diffusive, especially near the shock. One possible improvement is that instead of (3.10), we use the following three points discretization

$$\rho_{\epsilon j}^{n+1}-\frac{(1-\alpha\epsilon^2)\Delta t^2}{\epsilon^2\Delta x^2}\Big(p'(\rho_{\epsilon j+1}^n)\big(\rho_{\epsilon j+1}^{n+1}-\rho_{\epsilon j}^{n+1}\big)-p'(\rho_{\epsilon j}^n)\big(\rho_{\epsilon j}^{n+1}-\rho_{\epsilon j-1}^{n+1}\big)\Big)=D\phi(\rho_\epsilon^n,q_\epsilon^n). \tag{3.11}$$

The second term of (3.11) leads to a first order approximation of $\partial_{xx}p(\rho)$ which is in conservative form and consequently, will generate a consistent approximation of the shock speeds. Using a higher order approximation is unnecessary since the other parts of the scheme are also first order. After obtaining ρ_ϵ^{n+1}, we can substitute it into (3.7) to get $q_{\epsilon j}^{n+1}$.

To summarize, three schemes are proposed here: (3.8), (3.7); (3.10), (3.7) and (3.11), (3.7). To investigate the AP property, we take (3.7) and (3.10) as an example. The proofs for the other two schemes are similar. By substituting the following expansion

$$\rho_{\epsilon j}^n=\rho_{(0)c}^n+\epsilon^2\rho_{(2)j}^n+\cdots,\qquad q_{\epsilon j}^n=q_{(0)c}^n+\epsilon q_{(2)j}^n+\cdots, \tag{3.12}$$

into (3.10), the $\mathcal{O}(1/\epsilon^2)$ terms give that $\rho_{(0)j}^{n+1}=\rho_{(0)c}^{n+1}$ is constant in space by using the periodic boundary condition, and thus:

$$\rho_{\epsilon j}^{n+1}=\rho_{(0)c}^{n+1}+\epsilon^2\rho_{(2)j}^{n+1}+\cdots.$$

Summing (3.10) over all the grid points, one gets

$$\rho_{(0)c}^{n+1}=\rho_{(0)c}^n=\rho_{(0)c}, \tag{3.13}$$

which implies that ρ_0 is independent of time and space. Thus, the $\mathcal{O}(1)$ terms of (3.10) are

$$p'(\rho_{(0)c}^n)\big(\rho_{(2)j+2}^{n+1}-\rho_{(2)j}^{n+1}\big)-p'(\rho_{(0)c}^n)\big(\rho_{(2)j}^{n+1}-\rho_{(2)j-1}^{n+1}\big)=0,$$

by recalling that the $\mathcal{O}(1)$ terms of both ρ_ϵ^n and $\mathbf{q}_\epsilon^n$ are constant in space. Then the periodic boundary condition gives

$$\rho_{(2)j}^{n+1}=\rho_{(2)c}^{n+1}, \tag{3.14}$$

which gives that $\rho_{(2)}^{n+1}$ is also independent of space. Therefore from (1.2) and (3.7),

$$q_{(0)j}^{n+1}=q_{(0)j}^{n}=q_{(0)c}^{n}. \tag{3.15}$$

In one dimension, (3.13) is the discretization of (2.8), (2.9) and (2.11) when periodic boundary conditions apply and thus is consistent with the incompressible limit. In fact all the three methods proposed here are AP.

4 Full time and space discretization: two dimensional case

We consider the domain $\Omega=[0,1]\times[0,1]$. For M_1,M_2 two positive integers, we use a uniform spatial mesh $\Delta x=1/M_1$, $\Delta y=1/M_2$. The grid points are

$$(x_i,y_j)=(i\Delta x,j\Delta y),\quad i=0,\cdots,M_1;\ j=0,\cdots,M_2.$$

Now

$$U=(\rho_\epsilon,\rho_\epsilon u_{\epsilon 1},\rho_\epsilon u_{\epsilon 2})^T=(\rho_\epsilon,q_{\epsilon 1},q_{\epsilon 2})^T,$$

and $U_{i,j}$ is the numerical approximation of $U(x_i,y_j)$. Let

$$G_1(U)=\begin{pmatrix}\rho_\epsilon u_{\epsilon 1}\\ \rho_\epsilon u_{\epsilon 1}^2+\alpha p(\rho_\epsilon)\\ \rho_\epsilon u_{\epsilon 1}u_{\epsilon 2}\end{pmatrix},\quad G_2(U)=\begin{pmatrix}\rho_\epsilon u_{\epsilon 2}\\ \rho_\epsilon u_{\epsilon 1}u_{\epsilon 2}\\ \rho_\epsilon u_{\epsilon 2}^2+\alpha p(\rho_\epsilon)\end{pmatrix}, \tag{4.1}$$

$$Q=\frac{1-\alpha\epsilon^2}{\epsilon^2}\begin{pmatrix}0&0&0\\ \partial_x p&0&0\\ \partial_y p&0&0\end{pmatrix}.$$

Eq. (2.12) can be written as

$$\partial_t U+\partial_x G_1(U)+\partial_y G_2(U)+QU=0.$$

Denote

$$G_1(U^{n+\frac{1}{2}})=\begin{pmatrix}(\rho_\epsilon u_{\epsilon 1})^{n+1}\\ \rho_\epsilon^n(u_{\epsilon 1}^n)^2+\alpha p(\rho_\epsilon^n)\\ \rho_\epsilon^n u_{\epsilon 1}^n u_{\epsilon 2}^n\end{pmatrix},\quad G_2(U^{n+\frac{1}{2}})=\begin{pmatrix}(\rho_\epsilon u_{\epsilon 2})^{n+1}\\ \rho_\epsilon^n u_{\epsilon 1}^n u_{\epsilon 2}^n\\ \rho_\epsilon^n(u_{\epsilon 2}^n)^2+\alpha p(\rho_\epsilon^n)\end{pmatrix},$$

and

$$\tilde{Q}_{ij}=\begin{pmatrix} 0 & 0 & 0 \\ \frac{1-\alpha\epsilon^2}{\epsilon^2}D^x_{ij}\hat{p} & 0 & 0 \\ \frac{1-\alpha\epsilon^2}{\epsilon^2}D^y_{ij}\hat{p} & 0 & 0 \end{pmatrix},$$

with $\hat{p}(\rho_\epsilon)=p(\rho_\epsilon)$ an operator of ρ_ϵ and

$$D^x_{ij}u=\frac{u_{i+1j}-u_{i-1j}}{2\Delta x}, \qquad D^y_{ij}u=\frac{u_{ij+1}-u_{ij-1}}{2\Delta y}.$$

Now the eigenvalues of the two one dimensional Jacobians are

$$\lambda^{(1)}=u_{\epsilon 1},u_{\epsilon 1}\pm\sqrt{\alpha p'(\rho_\epsilon)}, \qquad \lambda^{(2)}=u_{\epsilon 2},u_{\epsilon 2}\pm\sqrt{\alpha p'(\rho_\epsilon)}.$$

The fully discrete scheme for the two dimensional problem is

$$\begin{aligned}&\frac{U^{n+1}_{ij}-U^n_{ij}}{\Delta t}+D^x_{ij}G_1(U^{n+1/2})+\frac{1}{2}\big(A_{i-\frac{1}{2},j}D^x_{ij-}-A_{i+\frac{1}{2},j}D^x_{ij+}\big)U^n\\ &\quad+D^y_{ij}G_2(U^{n+1/2})+\frac{1}{2}\big(A_{i,j-\frac{1}{2}}D^y_{ij-}-A_{i,j+\frac{1}{2}}D^y_{ij+}\big)U^n+\tilde{Q}_{ij}U^{n+1}=0,\end{aligned} \tag{4.2}$$

where

$$D^x_{ij-}u=\frac{u_{ij}-u_{i-1j}}{\Delta x}, \qquad D^x_{ij+}u=\frac{u_{i+1j}-u_{ij}}{\Delta x}, \tag{4.3a}$$

$$D^y_{ij-}u=\frac{u_{ij}-u_{ij-1}}{\Delta y}, \qquad D^y_{ij+}u=\frac{u_{ij+1}-u_{ij}}{\Delta y}, \tag{4.3b}$$

$$A^n_{i+\frac{1}{2},j}=\max\big\{|\lambda^{(1)}_{ij}|,|\lambda^{(1)}_{i+1,j}|\big\}, \qquad A^n_{i,j+\frac{1}{2}}=\max\big\{|\lambda^{(1)}_{ij}|,|\lambda^{(1)}_{i,j+1}|\big\}. \tag{4.3c}$$

Expressing $\mathbf{q}_\epsilon=(q_{\epsilon 1},q_{\epsilon 2})^T$ like in (3.7), similar as in one dimension, we can substitute the expressions of $q^{n+1}_{\epsilon 1ij},q^{n+1}_{\epsilon 2ij}$ into the density equation and get the following discretized elliptic equation

$$\begin{aligned}&\rho^{n+1}_{\epsilon ij}-\frac{(1-\alpha\epsilon^2)\Delta t^2}{4\epsilon^2}\Big(\frac{1}{\Delta x^2}\big(p(\rho^{n+1}_{\epsilon i+2,j})-2p(\rho^{n+1}_{\epsilon i,j})+p(\rho^{n+1}_{\epsilon i-2,j})\big)\\ &\quad+\frac{1}{\Delta y^2}\big(p(\rho^{n+1}_{\epsilon i,j+2})-2p(\rho^{n+1}_{\epsilon i,j})+p(\rho^{n+1}_{\epsilon i,j-2})\big)\Big)=D\phi_{ij}(\rho^n_\epsilon,q^n_{1\epsilon},q^n_{2\epsilon}),\end{aligned} \tag{4.4}$$

where

$$\begin{aligned}D\phi_{ij}(\rho_\epsilon^n,q_{\epsilon1}^n,q_{\epsilon2}^n)=&\rho_\epsilon^n-\Delta t\Big(D_{ij}^x q_{\epsilon1}^n+D_{ij}^y q_{\epsilon2}^n+\frac{1}{2}\big(A_{i-\frac{1}{2}}D_{ij-}^x-A_{i+\frac{1}{2},j}D_{ij+}^x\\&+A_{i,j-\frac{1}{2}}D_{ij-}^y-A_{i,j+\frac{1}{2}}D_{ij+}^y\big)\rho_\epsilon^n\Big)+\Delta t^2\Big(D_{ij}^xD_{ij}^x\big(\rho_\epsilon^n(u_{\epsilon1}^n)^2\\&+\alpha p(\rho_\epsilon^n)\big)+D_{ij}^yD_{ij}^y\big(\rho_\epsilon^n(u_{\epsilon2}^n)^2+\alpha p(\rho_\epsilon^n)\big)+(D_{ij}^xD_{ij}^y\\&+D_{ij}^yD_{ij}^x)\rho_\epsilon^nu_{\epsilon1}^nu_{\epsilon2}^n+\frac{1}{2}D_{ij}^x(A_{i-\frac{1}{2},j}D_{ij-}^x-A_{i+\frac{1}{2},j}D_{ij+}^x)q_{\epsilon1}^n\\&+\frac{1}{2}D_{ij}^y(A_{i-\frac{1}{2},j}D_{ij-}^x-A_{i+\frac{1}{2},j}D_{ij+}^x)q_{\epsilon2}^n+\frac{1}{2}D_{ij}^x(A_{i,j-\frac{1}{2}}D_{ij-}^y\\&-A_{i,j+\frac{1}{2}}D_{ij+}^y)q_{\epsilon1}^n+\frac{1}{2}D_{ij}^y(A_{i,j-\frac{1}{2}}D_{ij-}^y-A_{i,j+\frac{1}{2}}D_{ij+}^y)q_{\epsilon2}^n\Big).\end{aligned}\tag{4.5}$$

After obtaining ρ_{ij}^{n+1} by (4.4), $q_{\epsilon1ij}^{n+1},q_{\epsilon2ij}^{n+1}$ can be computed by the momentum equation afterwards.

Similar to the one-dimensional case, the modified diffusion operator using a reduced stencil is as follows:

$$\begin{aligned}&\rho_{\epsilon ij}^{n+1}-\Delta t^2\frac{1-\alpha\epsilon^2}{\epsilon^2}\times\Big[\frac{1}{\Delta x^2}\Big(p'(\rho_{\epsilon i,j+1}^n)(\rho_{\epsilon i,j+1}^{n+1}-\rho_{\epsilon i,j}^{n+1})-p'(\rho_{\epsilon i,j}^n)(\rho_{\epsilon i,j}^{n+1}-\rho_{\epsilon i,j-1}^{n+1})\Big)\\&\quad+\frac{1}{\Delta y^2}\Big(p'(\rho_{\epsilon i+1,j}^n)(\rho_{\epsilon i+1,j}^{n+1}-\rho_{\epsilon i,j}^{n+1})-p'(\rho_{\epsilon i,j}^n)(\rho_{\epsilon i,j}^{n+1}-\rho_{\epsilon i-1,j}^{n+1})\Big)\Big]\\&=D\phi(\rho_\epsilon^n,q_{\epsilon1}^n,q_{\epsilon2}^n).\end{aligned}\tag{4.6}$$

Now we prove the AP property of our fully discrete scheme. Here only well-prepared initial conditions are considered, which means that there will be no shock forming in the solution. Then α can be chosen to be 0 to minimize the introduced numerical viscosity. Assuming that the expansions of $\rho_\epsilon,\mathbf{u}_\epsilon$ in (2.5) hold at time t^n, when $\epsilon\to0$, the $\mathcal{O}(1/\epsilon^2)$ terms of (4.6) give

$$\begin{aligned}&\frac{1}{\Delta x^2}\Big(p'(\rho_{(0)i,j+1}^n)(\rho_{(0)i,j+1}^{n+1}-\rho_{(0)i,j}^{n+1})-p'(\rho_{(0)i,j}^n)(\rho_{(0)i,j}^{n+1}-\rho_{(0)i,j-1}^{n+1})\Big)\\&\quad+\frac{1}{\Delta y^2}\Big(p'(\rho_{(0)i+1,j}^n)(\rho_{(0)i+1,j}^{n+1}-\rho_{(0)i,j}^{n+1})-p'(\rho_{(0)i,j}^n)(\rho_{(0)i,j}^{n+1}-\rho_{(0)i-1,j}^{n+1})\Big)=0.\end{aligned}\tag{4.7}$$

When using periodic boundary conditions, one gets $\rho_{(0)ij}^{n+1}=\rho_{(0)c}^{n+1}$ from (1.2). The time independence of $\rho_{(0)}^{n+1}$, similar to the one dimensional case, can be obtained by summing (4.6) over all the grid points. Accordingly we have

$$\rho_{\epsilon ij}^{n+1}=\rho_{(0)c}^n+\epsilon^2\rho_{(2)ij}^{n+1}+\cdots.\tag{4.8}$$

To prove the limiting behavior of $\mathbf{u}_{\epsilon1},\mathbf{u}_{\epsilon2}$, we do not want to use the density equation because the diffusion operator with reduced stencil does not allow us to find the

corresponding density equation. Therefore, we consider the $\mathcal{O}(1)$ term of (4.6),

$$\begin{aligned}&\rho^{n+1}_{(0)ij}-\Delta t^2\times\Big[\frac{1}{\Delta x^2}\Big(p'(\rho^n_{(0)c})(\rho^{n+1}_{(2)i+1,j}-\rho^{n+1}_{(2)i,j})-p'(\rho^n_{(0)c})(\rho^{n+1}_{(2)i,j}-\rho^{n+1}_{(2)i-1,j})\Big)\\&\quad+\frac{1}{\Delta y^2}\Big(p'(\rho^n_{(0)c})(\rho^{n+1}_{(2)i,j+1}-\rho^{n+1}_{(2)i,j})-p'(\rho^n_{(0)c})(\rho^{n+1}_{(2)i,j}-\rho^{n+1}_{(2)i,j-1})\Big)\Big]\\&=D\phi(\rho^n_{(0)},q^n_{(0)1},q^n_{(0)2}).\end{aligned}\tag{4.9}$$

Moreover, noting the fact that

$$\begin{aligned}D^x_{ij}p(\rho^{n+1}_\epsilon)&=D^x_{ij}p(\rho^n_{(0)c}+\epsilon^2\rho^{n+1}_{(2)}+o(\epsilon^2))\\&=D^x_{ij}p(\rho^n_{(0)c})+\epsilon^2D^x_{ij}(\rho^{n+1}_{(2)}p'(\rho^n_{(0)c}))+o(\epsilon^2)\\&=\epsilon^2D^x_{ij}(\rho^{n+1}_{(2)}p'(\rho^n_{(0)c}))+o(\epsilon^2),\end{aligned}\tag{4.10}$$

and similarly,

$$D^y_{ij}p(\rho^{n+1}_\epsilon)=\epsilon^2D^y_{ij}(\rho^{n+1}_{(2)}p'(\rho^n_{(0)c}))+o(\epsilon^2),$$

the $\mathcal{O}(1)$ terms of the momentum equations of (4.2) become

$$\begin{aligned}&\frac{q^{n+1}_{(0)1ij}-q^n_{(0)1ij}}{\Delta t}+D^x_{ij}\Big(\frac{q^2_{(0)1}}{\rho_0}\Big)^n+D^y_{ij}\Big(\frac{q_{(0)1}q_{(0)2}}{\rho_0}\Big)^n+\frac{1}{2}\big(A_{i-\frac12,j}D^x_{ij-}-A_{i+\frac12,j}D^x_{ij+}\\&\qquad+A_{i,j-\frac12}D^y_{ij-}-A_{i,j+\frac12}D^y_{ij+}\big)\mathbf{q}_{01}=D^x_{ij}(p'(\rho^{n+1}_{(0)c})\rho^{n+1}_{(2)}),\end{aligned}\tag{4.11a}$$

$$\begin{aligned}&\frac{q^{n+1}_{(0)2ij}-q^n_{(0)2ij}}{\Delta t}+D^x_{ij}\Big(\frac{q_{(0)1}q_{(0)2}}{\rho_0}\Big)^n+D^y_{ij}\Big(\frac{q^2_{(0)2}}{\rho_0}\Big)^n+\frac{1}{2}\big(A_{i-\frac12,j}D^x_{ij-}-A_{i+\frac12,j}D^x_{ij+}\\&\qquad+A_{i,j-\frac12}D^y_{ij-}-A_{i,j+\frac12}D^y_{ij+}\big)q_{(0)2}=D^y_{ij}(p'(\rho^{n+1}_{(0)c})\rho^{n+1}_{(2)}).\end{aligned}\tag{4.11b}$$

Comparing (4.9) with $\Delta t*(D^x_{ij}(4.11a)+D^y_{ij}(4.11b))$, one gets

$$D^x_{ij}q^{n+1}_{(0)1}+D^y_{ij}q^{n+1}_{(0)2}=\mathcal{O}(\Delta x\Delta t),\tag{4.12}$$

which is an approximation of (2.9). Moreover, it is obvious that (4.11) is a discretization of (2.11). Thus we obtain a full discretization of (1.4) in the limit $\epsilon\to0$. Therefore, the two-dimensional scheme is also AP.

Remark 4.1. Defining a discrete curl of a vector q by $D^x_{ij}q_2-D^y_{ij}q_1$, we find that the discrete curl of the right-hand side of (4.11a) and (4.11b) is zero. Since the last term of the left-hand side is $\mathcal{O}(\Delta x)$, and since the leading order density is uniform (see (4.8)), Eqs. (4.11a) and (4.11b) express that the discrete convection operator applied to the velocity vector u is the discrete gradient of a vector field up to terms of order $\mathcal{O}(\Delta x)$. Therefore, the incompressible limit of the discrete system has the same structure as the continuous incompressible Euler equations.

5 Choice of the parameter α

Numerically, we find some nonphysical oscillations when $\alpha=0$. These oscillations can even be more severe when the time-step Δt is reduced and are produced by too small a numerical diffusion. Increasing the numerical diffusion motivates the explicit-implicit decomposition of the pressure term, which is controlled by the parameter α. In this section, we illustrate how to choose Δt and the parameter α by considering the simple state equation

$$p(\rho_\epsilon)=\rho_\epsilon. \tag{5.1}$$

In this context, the fully discrete scheme (3.4) in one dimension can be written as

$$\begin{cases} \dfrac{\rho_{\epsilon j}^{n+1}-\rho_{\epsilon j}^{n}}{\Delta t}+D_j^x(q_\epsilon^{n+1}-q_\epsilon^n)+F_{\rho_\epsilon j}^n=0, \\ \dfrac{q_\epsilon^{n+1}-q_\epsilon^n}{\Delta t}+F_{q_\epsilon j}^n+\dfrac{1-\alpha\epsilon^2}{\epsilon^2}D_j^x\rho_\epsilon^{n+1}=0, \end{cases} \tag{5.2}$$

where D_j^x is the centered difference (3.5a). By substituting $D_j^x\left(q_\epsilon^{n+1}-q_\epsilon^n\right)$ from the second equation of (5.2) into the first one, one gets Eqs. (3.8) and (3.9).

Let us consider the density equation (3.8), (3.9) for instance. The two terms

$$-\frac{(1-\alpha\epsilon^2)\Delta t}{4\epsilon^2\Delta x^2}\left(\rho_{\epsilon j+2}^{n+1}-2\rho_{\epsilon j}^{n+1}+\rho_{\epsilon j-2}^{n+1}\right), \qquad -\Delta t D_j^x F_{q_\epsilon} \tag{5.3}$$

behave like additional diffusion terms which stabilize the scheme even for large time steps. In order to quantify these diffusion terms, we compare with a standard explicit Rusanov scheme. We refer to [21] for a general discussion of numerical viscosity.

For simplicity, we first consider a scalar hyperbolic equation

$$\partial_t u+\partial_x f(u)=0.$$

The corresponding explicit Rusanov scheme is

$$\frac{u_j^{n+1}-u_j^n}{\Delta t}+\frac{Fu_{j+\frac12}^n-Fu_{j-\frac12}^n}{\Delta x}=0, \tag{5.4}$$

where $Fu_{j+1/2}$ is the numerical flux as follows

$$Fu_{j+\frac12}^n=\frac12\left(Fu_{j+\frac12}^{n+}+Fu_{j-\frac12}^{n-}\right)=\frac12\left(f(u_{j+1}^n)+f(u_j^n)\right)-\frac12A_{j+\frac12}^n(u_{j+1}^n-u_j^n),$$

where

$$\begin{aligned} &Fu_{j+\frac12}^{n+}=f(u_j^n)+A_{j+\frac12}^n u_j^n, \qquad Fu_{j+\frac12}^{n-}=f(u_{j+1}^n)-A_{j+\frac12}^n u_{j+1}^n, \\ &A_{j+\frac12}^n=\max\left\{|f'(u_j^n)|,|f'(u_{j+1}^n)|\right\}. \end{aligned} \tag{5.5}$$

Let

$$A=\max\left\{\left|f'\left(u\left(x-\frac{\Delta x}{2}\right)\right)\right|,\left|f'\left(u\left(x+\frac{\Delta x}{2}\right)\right)\right|\right\}.$$

The local truncation error of the flux Fu at $x+\Delta x/2$ is:

$$LFu=f(u)-\frac{\Delta x}{2}Au_x+\mathcal{O}(\Delta x^2),$$

and that of (5.4) becomes

$$L(x,t)=u_t+\frac{\Delta t}{2}u_{tt}+(f(u))_x-\frac{\Delta x}{2}(Au_x)_x+\mathcal{O}(\Delta x^2)+\mathcal{O}(\Delta t^2). \tag{5.6}$$

Comparing with the standard space-centered finite difference discretization, which is known to be unstable, the diffusion term

$$-\frac{\Delta x}{2}(Au_x)_x$$

has the effect of stabilizing the scheme.

We now use this analysis and postulate that our semi-implicit scheme is stable as soon as its numerical viscosity is larger than that of the standard Rusanov scheme (of course, it is only a sufficient condition, not a necessary one). By extending the previous analysis to the Isentropic Euler equations (1.1) in one space dimension, the standard Rusanov scheme leads to diffusion terms respectively equal to

$$\frac{\Delta x}{2}\partial_x\left(\left(|u_\epsilon^n|+\frac{1}{\epsilon}\right)\partial_x\rho_\epsilon^n\right)\quad\text{and}\quad\frac{\Delta x}{2}\partial_x\left(\left(|u_\epsilon^n|+\frac{1}{\epsilon}\right)\partial_x q_\epsilon^n\right), \tag{5.7}$$

for the mass and momentum equations.

Let us now consider the AP-scheme (5.2). We first consider the diffusion for the density equation. There are two diffusion terms which come from the $\mathcal{O}(\Delta t)$ terms (5.3) and which can be written as

$$-\Delta t\frac{1-\alpha\epsilon^2}{\epsilon^2}\partial_{xx}\rho_\epsilon^{n+1}+\mathcal{O}(\Delta t\Delta x),\qquad -\Delta t\partial_{xx}\left(\frac{q_\epsilon^{n2}}{\rho_\epsilon^n}+\alpha\rho_\epsilon^n\right)+\mathcal{O}(\Delta t\Delta x).$$

A third one is encompassed in $D_j^x F_{\rho_\epsilon}$, and is equal to

$$-\frac{\Delta x}{2}\partial_x\left((|u_\epsilon^n|+\sqrt{\alpha})\partial_x\rho_\epsilon^n\right)$$

(plus higher order terms, according to the previous analysis, and the fact that the viscosity terms for the AP scheme are given by (3.2) and (3.3)). By noting that

$$\rho_\epsilon^{n+1}=\rho_\epsilon^n-\Delta t D_j^x q_\epsilon^{n+1}+\mathcal{O}(\Delta t\Delta x), \tag{5.8}$$

then

$$-\Delta t\frac{1-\alpha\epsilon^2}{\epsilon^2}\partial_{xx}\rho_\epsilon^{n+1}-\Delta t\partial_{xx}(\alpha\rho_\epsilon^n)=-\frac{\Delta t}{\epsilon^2}\partial_{xx}\rho_\epsilon^n-\frac{1}{\epsilon^2}\mathcal{O}(\Delta t^2).$$

The diffusion terms for ρ_ϵ now is

$$\frac{\Delta x}{2}\partial_x\big((|u_\epsilon^n|+\sqrt{\alpha})\partial_x\rho_\epsilon\big)+\frac{\Delta t}{\epsilon^2}\partial_{xx}\rho_\epsilon^n+\Delta t\partial_{xx}(\rho_\epsilon^n u_\epsilon^{n2}) \tag{5.9}$$

plus some higher order terms.

Now, we focus on the momentum equation. From (5.8), the diffusion for q_ϵ is

$$\frac{\Delta x}{2}\partial_x\big((|u_\epsilon^n|+\sqrt{\alpha})\partial_x q_\epsilon^n\big)+\Delta t\frac{1-\alpha\epsilon^2}{\epsilon^2}\partial_{xx}q_\epsilon^n \tag{5.10}$$

plus some higher order terms. Here (5.10) is a scalar in one dimension and a vector in higher dimension.

Now, we assume that a sufficient condition for stability of the AP-scheme is that

(i) the diffusion coefficients involved in (5.9) and (5.10) are larger than those involved in the classical Rusanov scheme (5.7),

(ii) the CFL condition for the explicit part of the scheme is satisfied.

Condition (i) leads to

$$\frac{1}{2}\big(|u_\epsilon^n|+\sqrt{\alpha}\big)\Delta x+\frac{1-\alpha\epsilon^2}{\epsilon^2}\Delta t\geq\frac{1}{2}\big(|u_\epsilon^n|+\frac{1}{\epsilon}\big)\Delta x,$$

that is

$$\Delta t\geq\frac{1}{2}\epsilon\Delta x\frac{1}{1+\sqrt{\alpha}\epsilon}. \tag{5.11}$$

Condition (ii) gives

$$\Delta t\leq\sigma\frac{\Delta x}{\max\big\{|u_\epsilon^n|+\sqrt{\alpha}\big\}}, \tag{5.12}$$

where σ is the Courant number which is 1 theoretically. Then the parameter α should satisfy

$$\frac{\Delta x}{2\Delta t}-\frac{1}{\epsilon}\leq\sqrt{\alpha}\leq\frac{\sigma\Delta x}{\Delta t}-\max\big\{|u_\epsilon^n|\big\} \tag{5.13}$$

according to (5.11) and (5.12). We note that this is possible only if the following constraint on Δt is satisfied

$$\max\big\{|u_\epsilon^n|\big\}+\frac{\Delta x}{2\Delta t}\leq\frac{\sigma\Delta x}{\Delta t}+\frac{1}{\epsilon}. \tag{5.14}$$

This condition suggests that we must restrict to Courant numbers $\sigma>0.5$ (in practice, we choose $\sigma=0.8$). Indeed, if $\sigma\leq0.5$, there are some situations where, whatever the choice of α, it is impossible to match (5.11), i.e., to produce enough numerical diffusion. These situations are those where $\max\big\{|u_\epsilon^n|\big\}>1/\epsilon$. So, this is why we choose $\sigma>0.5$, because,

with this choice, such a situation never occurs. Now, noting that $\alpha \leq 1/\epsilon^2$, the biggest possible α is

$$\min\left\{\frac{1}{\epsilon^2}, \left(\sigma\frac{\Delta x}{\Delta t} - \max|u_\epsilon^n|\right)^2\right\}. \tag{5.15}$$

If we determine α from (5.15) with $\sigma > 0.5$, Δt can always be small enough to make (5.14) hold. Note that the smallness condition on Δt does not destroy the AP character of the scheme because the required threshold for Δt deduced from (5.12) is obviously independent of ϵ when ϵ is small.

In summary, the strategy is to choose α according to (5.15). In the numerical tests, we exhibit the corresponding results by setting $\sigma = 0.8$. We will see that, when α is chosen according to this strategy, more dissipation is introduced when Δt becomes small and the oscillations are suppressed.

6 Numerical results

Three numerical examples will allow us to test the performances of the proposed schemes. In fact, three schemes are proposed in Sections 3 and 4, for example in one dimension: the scheme (3.4) without linearizing $\nabla p(\rho_\epsilon^{n+1})$ is denoted by "NL". We need to use Newton iterations to solve the nonlinear system. When $\nabla p(\rho_\epsilon^{n+1})$ is approximated by $p'(\rho_\epsilon^n)\nabla\rho_\epsilon^{n+1}$, the elliptic system becomes linear. This scheme is represented by "L". "LD" denotes the scheme with the narrower stencil (3.11). Here we use well-prepared initial conditions of the form (1.3) and give three examples, each having different purposes:

- Show the differences between the three schemes and investigate their stability and convergence. Test the effect of the parameter α by comparing to the ICE scheme and illustrate the advantage of the AP-property numerically. Finally give the properties of "LD" when α is chosen as in (5.15).
- Simulate the collision of two acoustic waves.
- Provide a two dimensional example.

In the one-dimensional case, let the computational domain be $[a,b]$ and the mesh size be Δx. The grid points are

$$x_j = a + (j-1)\Delta x.$$

In the following tables, the L^2 norm of the relative error between the reference solutions u and the numerical ones U

$$e(U) = \frac{\|U-u\|_{L^2}}{\|u\|_{L^2}} = \frac{\frac{1}{M}\left(\sum_j |U_j - u(x_j)|^2\right)^{\frac{1}{2}}}{\frac{1}{M_e}\left(\sum_i |u(x_i)|^2\right)^{\frac{1}{2}}}$$

are displayed.

Example 6.1. $p(\rho_\epsilon)$ and the initial conditions are chosen as chosen as

$$
\begin{aligned}
&p(\rho_\epsilon)=\rho_\epsilon^2,\\
&\rho_\epsilon(x,0)=1, \qquad q_\epsilon(x,0)=1-\frac{\epsilon^2}{2}, \quad x\in[0,0.2]\cup[0.8,1],\\
&\rho_\epsilon(x,0)=1+\epsilon^2, \quad q_\epsilon(x,0)=1, \qquad x\in(0.2,0.3],\\
&\rho_\epsilon(x,0)=1, \qquad q_\epsilon(x,0)=1+\frac{\epsilon^2}{2}, \quad x\in(0.3,0.7],\\
&\rho_\epsilon(x,0)=1-\epsilon^2, \quad q_\epsilon(x,0)=1, \qquad x\in(0.7,0.8].
\end{aligned}
$$

This example consists of several Riemann problems. Shocks and contact discontinuities are stronger when ϵ is bigger. We first check the different behaviours of the three schemes (3.8), (3.10) and (3.11) by setting $\alpha=1$. The CFL condition for the linearized reduced stencil scheme (3.11) is discussed in (ii) and a fixed Courant number independent of ϵ is found numerically. Compared with the first order ICE method using Rusanov discretization for (1.5a), the improvement resulting from the removal of nonphysical oscillation that our scheme produces is shown. We investigate the effect of α for different values of ϵ in (iii). In (iv), when $\alpha=1$, we numerically test the uniform convergence order. The AP property and its advantages are demonstrated in (v) by comparing with the fully explicit Rusanov scheme for the initial Isentropic Euler equations (1.1). Finally, in (vi) the strategy (5.15) for choosing α as a function of Δt is tested.

When $\epsilon=0.1$, the initial density and momentum are displayed in Fig. 1 and we can see the discontinuities clearly.

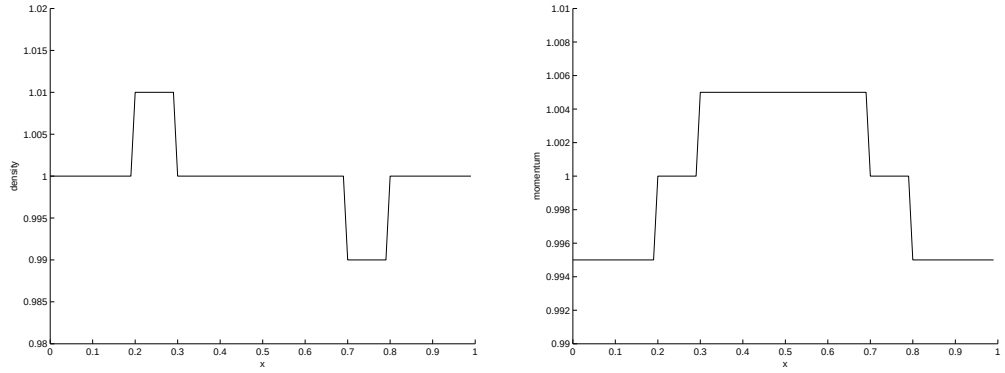

Figure 1: Example 6.1. When $\epsilon=0.1$, the initial density and momentum are displayed.

(i) In this example, we choose $\epsilon=0.8$, 0.3, 0.05 corresponding to the compressible, intermediate and incompressible regimes. Setting $\alpha=1$, the numerical results at $T=0.05$ of "NL", "L" and "LD" are represented in Fig. 2. Here Δt is chosen to make all these three schemes stable and diminishing Δt only will not improve much the numerical accuracy. The reference solution is calculated by an explicit Rusanov method [19,20] with $\Delta x=1/500, \Delta t=1/20000$. We can see that all these three methods can capture the right

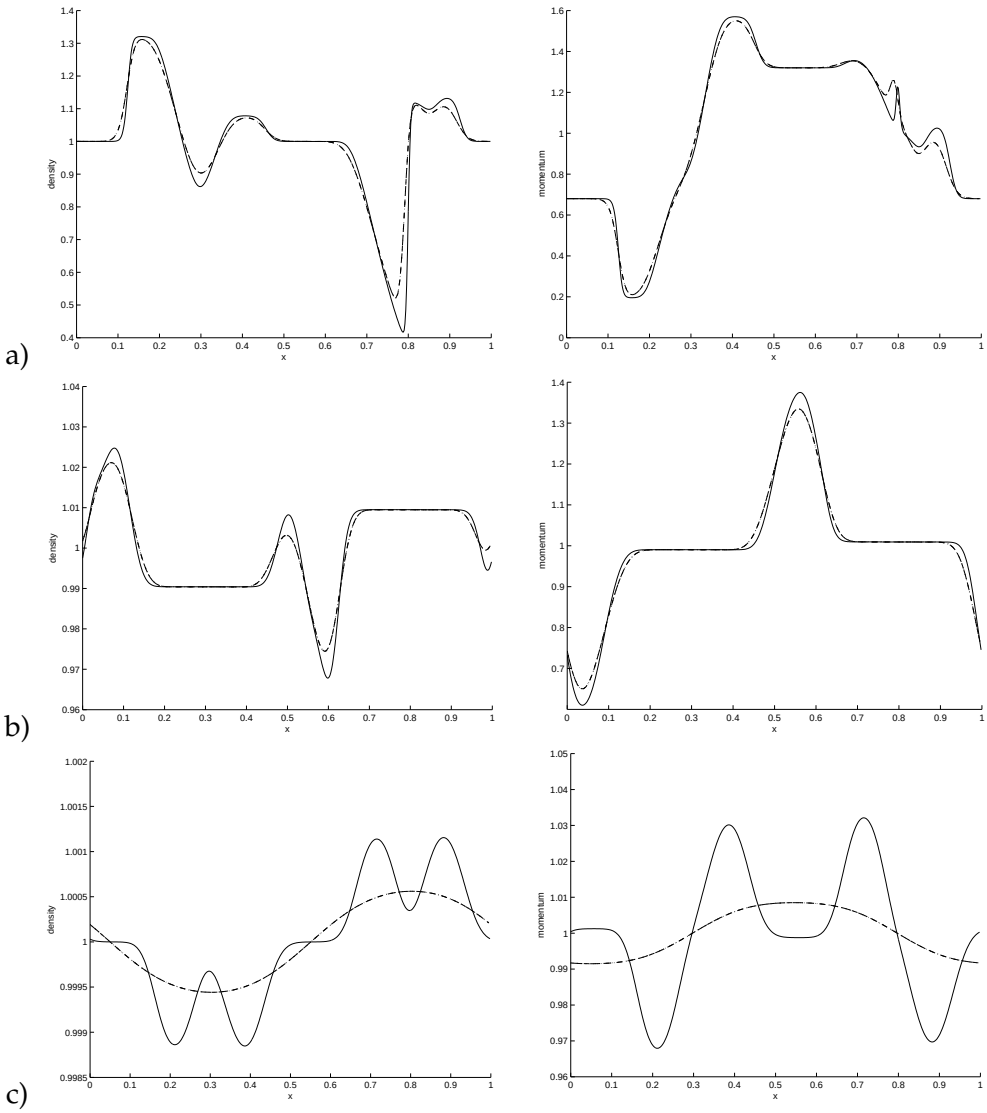

Figure 2: Example 6.1. When $T=0.05, \Delta x=1/200, \Delta t=1/2000$, the density and momentum of the "NL", "L" and "LD" schemes for the isentropic Euler equations are represented respectively by dashed, dash dotted, and dotted lines. The solid line is the reference solution calculated by an explicit Rusanov method [19, 20] with $\Delta x=1/500, \Delta t=1/20000$. a): $\epsilon=0.8$; b): $\epsilon=0.3$; c): $\epsilon=0.05$. Left: density; Right: momentum. For all ϵ's, these three lines are so close to each other that "-.-." and "..." are not visible in the figure.

shock speed. The results of the three schemes are quite close, which implies that the linearization idea does simplify the scheme but the "LD" scheme does not really introduce less diffusion. When ϵ is small, though we can no longer capture all the details of the waves, the error is of the order Δx which is the maximum information one can expect. Numerically, for different scales of ϵ, there is not much difference between these three

methods. Thus in the following one dimensional examples, we only test the performance of the "LD" scheme.

(ii) Because of the explicit treatment of the flux terms in the momentum equation, the stability of the "LD" scheme can be only guaranteed under the following CFL condition

$$\Delta t \leq \sigma \min_i \left\{ \frac{\Delta x}{|u_i| + \sqrt{\alpha p'(\rho_\epsilon)}} \right\}, \tag{6.1}$$

here $0 < \sigma < 1$ is the Courant number and is set up at initialization. Consistently with the fact that these three methods are AP, the Courant number does not depend on ϵ. Indeed, below, we numerically verify that σ is independent of ϵ. For $\epsilon = 0.8$, 0.3, 0.05, the numerical Courant numbers are displayed in Table 1 and we can see numerically that the biggest allowed $\max\{u\}\Delta t/\Delta x$ are close to 1 for all ϵ's. Therefore, $\sigma = 0.8$ is enough to guarantee stability and is numerically shown to be independent of ϵ. By contrast, the explicit Rusanov scheme for the original Euler equations has a stability condition which becomes more and more restrictive as ϵ goes to zero. Thus the CFL condition of the standard hyperbolic solver $\Delta t = \mathcal{O}(\epsilon \Delta x)$ is considerably improved.

Table 1: Example 6.1. The numerical Courant numbers for different ϵ. Here $\max\{\lambda\}$ denotes the maximum of $\max\{\lambda_j\}$ defined in (3.2) until $T = 0.1$ for all time steps.

ϵ	$\max\lambda$	Δx	stableΔt	$\frac{\Delta x}{\Delta t}$	$u\frac{\Delta t}{\Delta x}$
0.8	4.24	1/100	1/340	3.40	1.25
0.8	6.35	1/200	1/970	4.85	1.31
0.8	6.58	1/400	1/2420	6.05	1.09
0.8	6.70	1/800	1/5460	6.82	0.982
0.3	2.64	1/100	1/260	2.60	1.02
0.3	2.70	1/200	1/510	2.55	1.06
0.3	2.76	1/400	1/1000	2.50	1.10
0.3	2.81	1/800	1/2050	2.56	1.10
0.05	2.43	1/100	1/260	2.60	0.93
0.05	2.44	1/200	1/490	2.45	1.00
0.05	2.45	1/400	1/960	2.40	1.02
0.05	2.46	1/800	1/1920	2.40	1.03

(iii) The classical ICE method even in its conservative form introduces some non-physical oscillations, no matter how small the time step is. These oscillations cannot be diminished by decreasing the time step. Their amplitude becomes smaller as the mesh is refined as long as the scheme is stable. In this part we show that our method can suppress these oscillations numerically by choosing $\alpha = 1$. When $T = 0.01$, for $\epsilon = 0.8$, 0.3, 0.05, the numerical results of both our method with $\alpha = 1$ and ICE calculated by $\Delta x = 1/200, \Delta t = 1/20000$ are displayed in Fig. 3. The oscillations are more pronounced for the ICE method and are smoothed away when $\alpha = 1$. We can see that numerical nonphysical oscillations occur in the results of the ICE method when $\epsilon = 0.8$, 0.3, but disappear when ϵ becomes small. This can also be seen from (5.9) and (5.10). When ϵ is

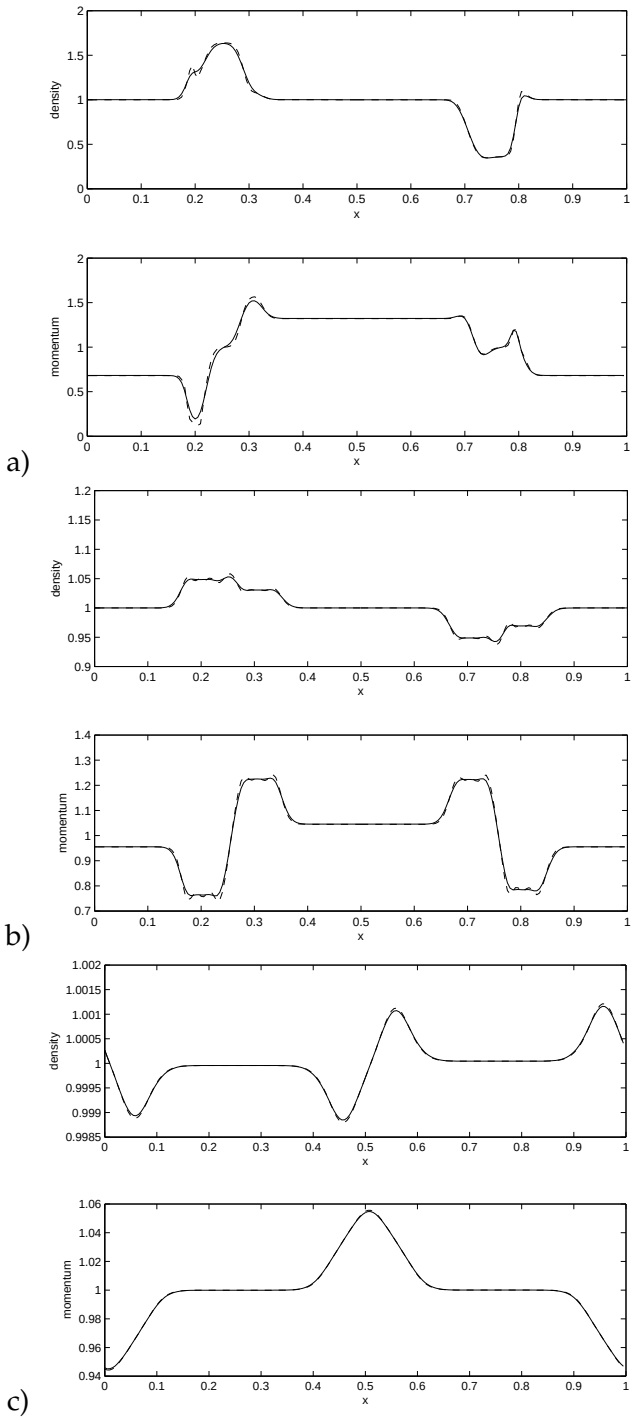

Figure 3: Example 6.1. When $T=0.01$, the density and momentum for different ϵ are presented. The solid and dashed lines are the numerical results of our scheme and the ICE method with $\Delta x=1/200$, $\Delta t=1/20000$ respectively. a): $\epsilon=0.8$; b): $\epsilon=0.3$; c): $\epsilon=0.05$.

small the diffusion introduced by the implicitness is bigger. These oscillations also go away as time goes on due to dissipation.

(iv) When $\alpha = 1$, the relative errors of the "LD" scheme for different Δx, Δt at time $T = 0.1$ are shown in Table 2. Here Δx, Δt do not need to resolve ϵ and the reference solution is obtained by the explicit Rusanov scheme calculated with a very fine mesh $\Delta x = 1/1280$, $\Delta t = 1/128000$. We can see that good numerical approximations can be obtained without resolving the small ϵ. The convergence order is $1/2$ when $\Delta t/\Delta x$ is fixed, uniformly with respect to ϵ. This convergence order when there are discontinuities is the same as the explicit Rusanov scheme [21]. We can see from Table 2 that refining the time step does not improve the accuracy much (provided the Courant number is appropriately small, like $\sigma = 0.8$). Take $\epsilon = 0.8$ as an example. When $\Delta x = 1/320$, in order to obtain stability, Δt should be less than $1/1920$. It is demonstrated in Table 2 that the error calculated with $\Delta x = 1/320$ does not decrease much when Δt is changed from $1/2880$ to $1/12800$. Thus as long as the scheme is stable, we cannot use a smaller Δt to obtain a better accuracy. This feature is the same as for standard hyperbolic solvers.

Table 2: Example 6.1. $T = 0.1$, the L^2 norm of the relative error between the reference solution which is calculated with a very fine mesh $\Delta x = 1/1280$, $\Delta t = 1/128000$ and the numerical results for different ϵ with different Δx,Δt are displayed.

ϵ	Δx	Δt	$e(\rho_\epsilon)$	ratio	$e(p_\epsilon)$	ratio
0.8	1/20	1/180	$9.739*10^{-1}$	-	1.197	-
0.8	1/40	1/360	$5.959*10^{-1}$	1.63	$7.484*10^{-1}$	1.16
0.8	1/80	1/720	$3.467*10^{-1}$	1.72	$4.180*10^{-1}$	1.31
0.8	1/160	1/1440	$1.985*10^{-1}$	1.75	$2.048*10^{-1}$	1.36
0.8	1/320	1/2880	$1.126*10^{-1}$	1.76	$8.477*10^{-2}$	1.79
0.8	1/320	1/12800	$1.126*10^{-1}$	-	$8.539*10^{-2}$	-
0.05	1/20	1/70	$4.679*10^{-3}$	-	$1.355*10^{-1}$	-
0.05	1/40	1/140	$3.305*10^{-3}$	1.42	$9.574*10^{-2}$	1.42
0.05	1/80	1/280	$2.353*10^{-3}$	1.40	$6.758*10^{-2}$	1.42
0.05	1/160	1/560	$1.655*10^{-3}$	1.42	$4.430*10^{-2}$	1.53
0.05	1/320	1/1120	$1.094*10^{-3}$	1.51	$2.538*10^{-2}$	1.75
0.05	1/320	1/12800	$6.012*10^{-4}$	-	$9.303*10^{-3}$	-

(v) In this part, we are concerned with the AP property. For $\epsilon = 0.005$, the numerical results at $T = 0.01$ with unresolved mesh $\Delta x = 1/20$, $\Delta t = 1/500$ and resolved mesh $\Delta x = 1/2000$, $\Delta t = 1/5000$ are displayed in Fig. 4, while the fully explicit Rusanov scheme is not stable with the same mesh size. We do capture the incompressible limit when Δx,Δt do not resolve ϵ.

(vi) Now we test the strategy (5.15) for choosing α. We set $\sigma = 0.8$. The numerical results at both the compressible and incompressible regimes for different values of Δt are displayed in Fig. 5. As for example (i), the reference solutions are calculated by an explicit Rusanov scheme with $\Delta x = 1/500$, $\Delta t = 1/20000$. We can see that the oscillations

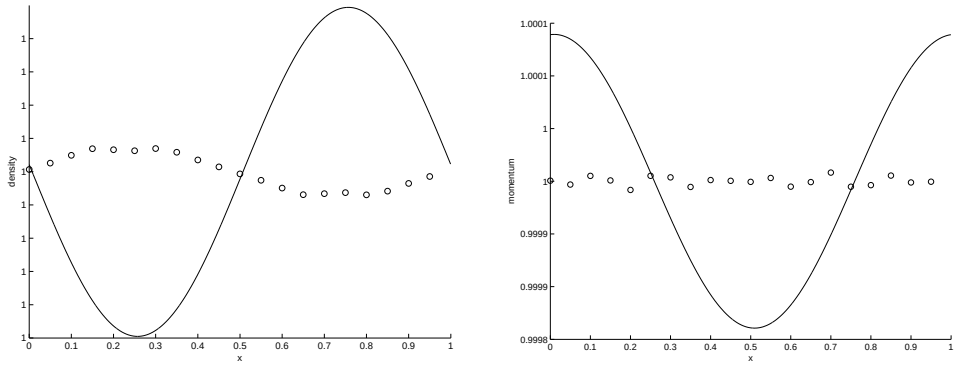

Figure 4: Example 6.1. By using the "LD" scheme, the density (left) and momentum (right) for $\epsilon=0.005$ at $T=0.01$ are represented. The circles are the results for $\Delta x=1/20$, $\Delta t=1/500$ and the solid line is calculated with $\Delta x=1/2000$, $\Delta t=1/5000$.

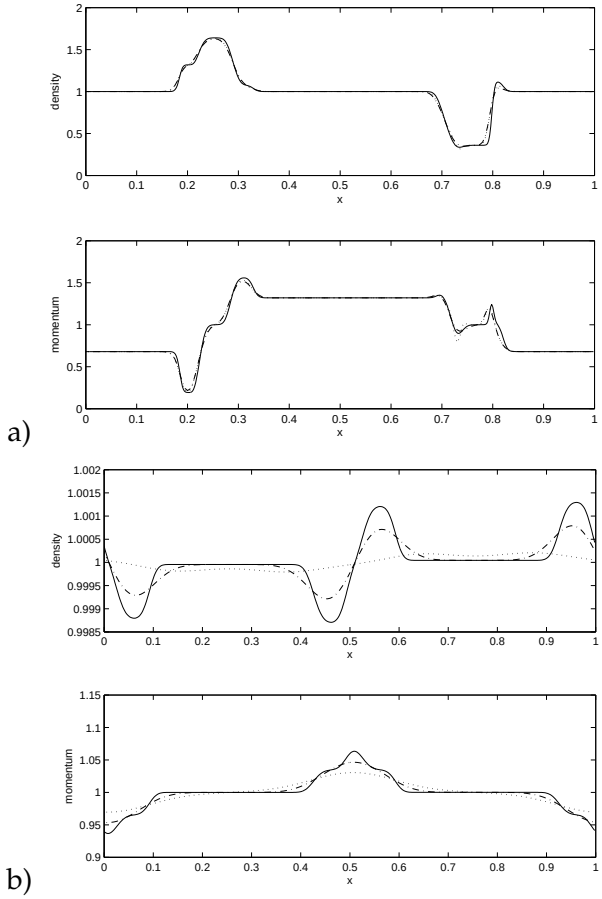

Figure 5: Example 6.1. By using the "LD" scheme, at $T=0.01$, the density and momentum for $\epsilon=0.8$ and 0.05 are presented. The dotted and dash dotted lines are the numerical results of $\Delta x=1/200$,$\Delta t=1/1000$ and $\Delta x=1/200$, $\Delta t=1/20000$ respectively and the solid lines represent the reference solution calculated by explicit Rusanov scheme with very fine mesh. a): $\epsilon=0.8$; b): $\epsilon=0.05$.

disappear as long as Δt is small enough to make the scheme stable. Moreover, it is easy to check that the explicit Rusanov scheme is no longer stable when $\epsilon=0.05$ and $\Delta x=1/200$, $\Delta t=1/1000$. Therefore, when we choose α as in (5.15), the oscillations are suppressed and the possibility of using large time and space steps (compared to ε) is preserved.

Example 6.2. In this example we simulate the evolution of two collision acoustic waves by the "LD" scheme and test the convergence. We choose $\alpha=1$, $\epsilon=0.1$, $\Delta x=1/100$, $\Delta t=1/1000$. Here Δt is chosen to stabilize the scheme and decreasing Δt alone will not improve much the numerical accuracy. Similar to Klein's paper [17], $p(\rho_\epsilon)$ and the initial conditions are chosen as

$$p(\rho_\epsilon)=\rho_\epsilon^{1.4},\quad \text{for } x\in[-1,1],$$
$$\rho_\epsilon(x,0)=0.955+\frac{\epsilon}{2}\big(1-\cos(2\pi x)\big),\qquad q_\epsilon(x,0)=-\text{sign}(x)\sqrt{1.4}\big(1-\cos(2\pi x)\big).$$

The initial density and momentum are displayed in Fig. 6.

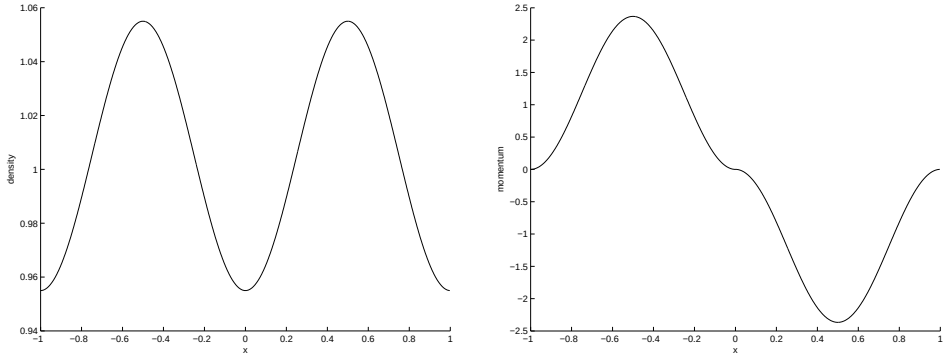

Figure 6: Example 6.2. When $\epsilon=0.1$, the initial density and momentum are displayed.

For $\epsilon=0.1$, the numerical results of the "LD" scheme at different times T are shown in Fig. 7. The initial data approximate two acoustic pulses, one right-running and one left-running. They collide and their superposition gives rise to a maximum in the density. Then the pulses separate again. This procedure is demonstrated clearly in Fig. 7.

Example 6.3. In this example, we show numerical results for the two dimensional case. Let $p(\rho)=\rho^2$, and the computational domain be $(x,y)\in[0,1]\times[0,1]$. Because no shock will form in this example, we choose $\alpha=0$ and the initial condition as follows:

$$\rho(x,y,0)=1+\epsilon^2\sin^2\big(2\pi(x+y)\big),$$
$$q_{\epsilon1}(x,y,0)=\sin\big(2\pi(x-y)\big)+\epsilon^2\sin\big(2\pi(x+y)\big),$$
$$q_{\epsilon2}(x,y,0)=\sin\big(2\pi(x-y)\big)+\epsilon^2\cos\big(2\pi(x+y)\big).$$

The initial conditions for $\epsilon=0.8$ and numerical results at $T=1$ calculated with $\Delta x=1/20$, $\Delta t=1/80$ are shown in Fig. 8. Numerical tests show that a similar CFL condition

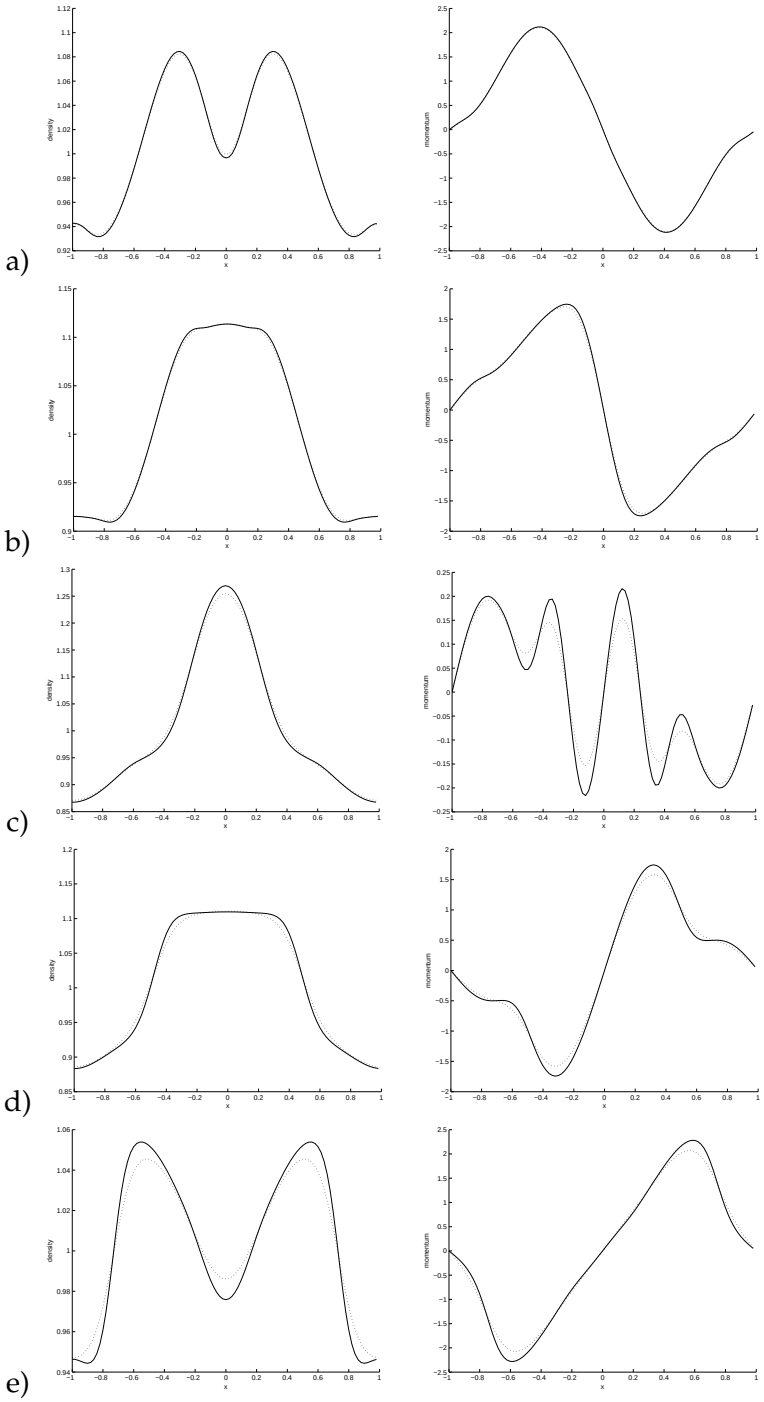

Figure 7: Example 6.2. When $\epsilon=0.1$, the density and momentum of the "LD" scheme at different times are represented: a): $T=0.01$; b): $T=0.02$; c): $T=0.04$; d): $T=0.06$; e): $T=0.08$. All these pictures correspond to $\Delta x=1/50$, $\Delta t=1/1000$.

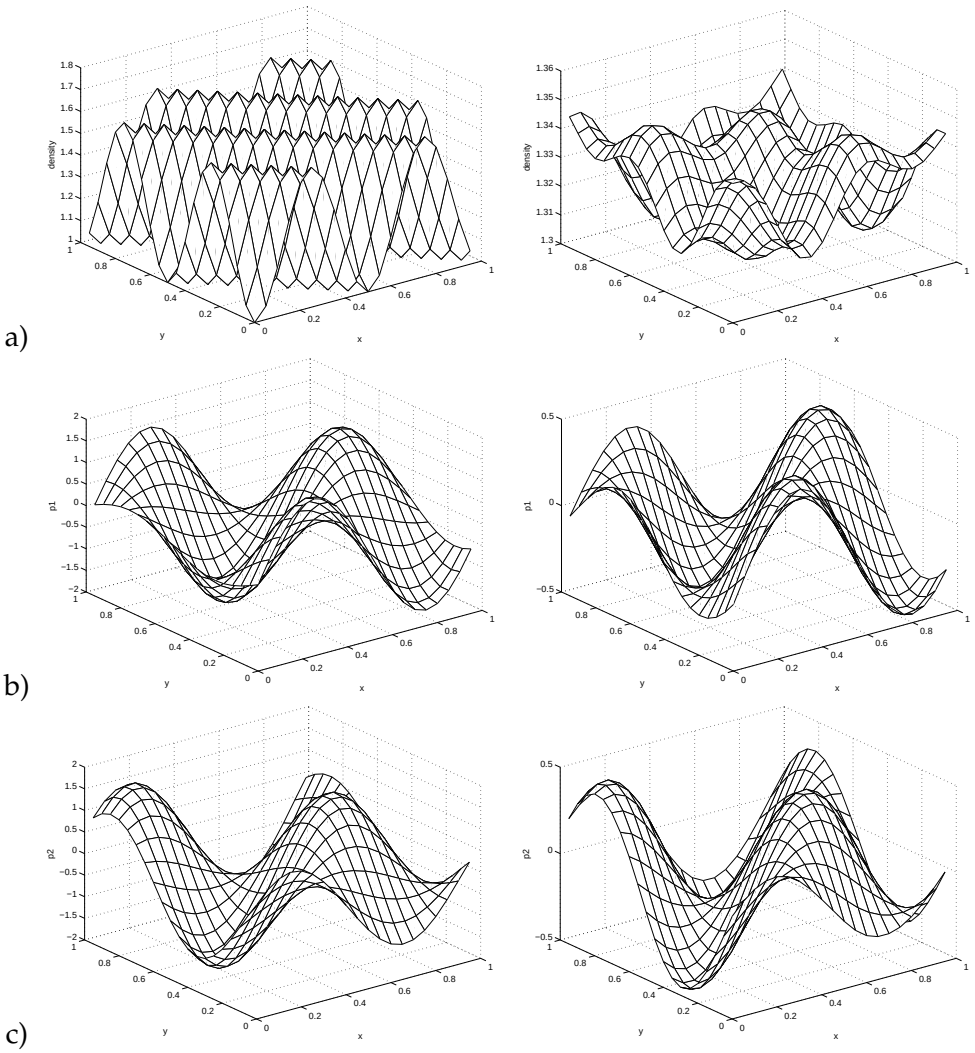

Figure 8: Example 6.3. When $\epsilon=0.8$, the initial density and momentum (left) and the numerical result with $\Delta x=1/20,\Delta t=1/80$ at time $T=1$ (right) are represented. a): ρ_ϵ; b): $q_{\epsilon 1}$; c): $q_{\epsilon 2}$.

is required as for the one-dimensional case. When $\epsilon=0.05$ at time $T=1$, the numerical results with an unresolved mesh Δx=1/20, Δt=1/80 and a resolved mesh Δx=1/80, Δt= 1/320 are displayed in Fig. 9. We can see that the results using the coarse mesh are much "smoother" than the one using the refined mesh. In this example the amplitude decay due to numerical diffusion cannot be ignored. When a coarse mesh is used, the first order method is known to have dissipation. This is mainly due to the numerical diffusion term, which smoothes out the solution. This phenomenon not only happens when ϵ is small but also when ϵ is $\mathcal{O}(1)$. We can also see from Fig. 9 that when ϵ is small, $D^x q_{\epsilon 1}+D^y q_{\epsilon 2}$ is close to 0.

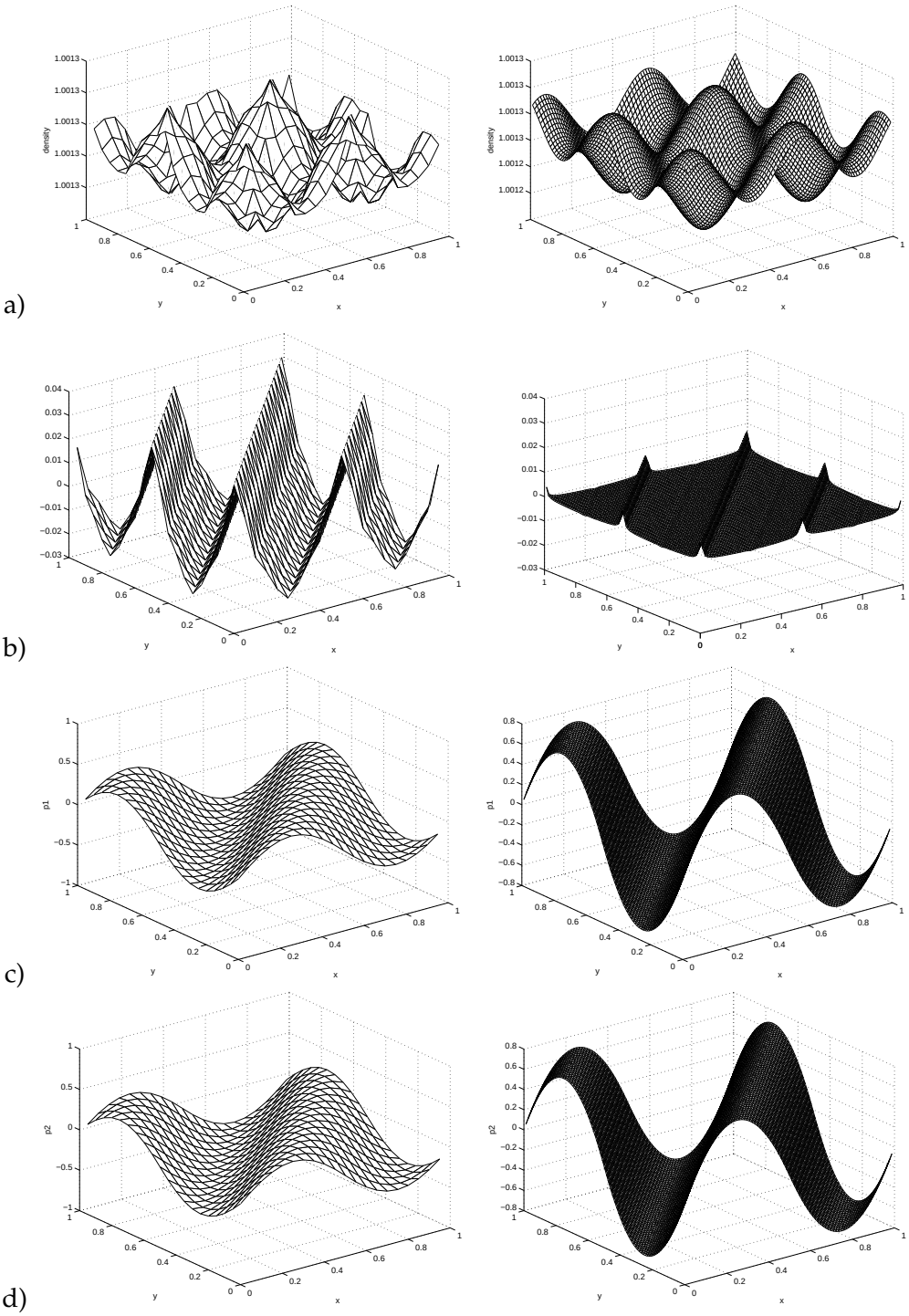

Figure 9: Example 6.3. When $\epsilon=0.05$, the numerical result with $\Delta x=1/20,\Delta t=1/80$ (left) and $\Delta x=1/80,\Delta t=1/320$ (right) at time $T=1$ are represented respectively. a): ρ_ϵ; b): $D^x q_{\epsilon 1}+D^y q_{\epsilon 2}$; c): $q_{\epsilon 1}$; d): $q_{\epsilon 2}$.

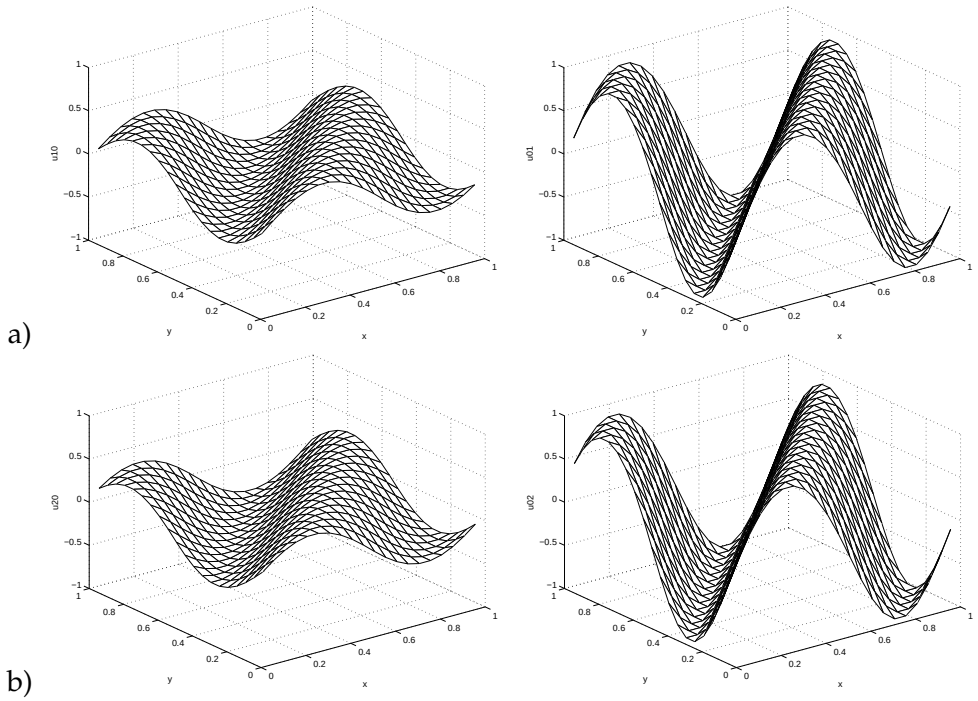

Figure 10: Example 6.3. The numerical results of the incompressible Euler limit using $\Delta x=1/20$,$\Delta t=1/80$ with (left) and without (right) viscosity at time $T=1$ are represented. a): the first element of the velocity $u_{(0)1}$; b): the second element of the velocity $u_{(0)2}$.

As a comparison, the numerical solutions of the incompressible limit (1.4) with and without numerical viscosity are shown in Fig. 10. The latter is obtained by a difference method based on a staggered grid configuration [13]. This staggered difference method is attractive for incompressible flows, since no artificial terms are needed to obtain stability and suppress the oscillations. Because of the stable pressure-velocity coupling, solutions with almost no viscosity can be obtained. The viscosity introduced here is of the form $A\Delta x/2$ where A is given by (4.3c). We can see that the amplitude of the wave decays as time evolves even though the viscosity is only $\mathcal{O}(\Delta x)$. In the limit of $\epsilon\to 0$, (4.11) generates a discretization of the incompressible limit with $\mathcal{O}(\Delta x)$ numerical diffusion terms. This is why the results for $\Delta x=1/20$, $\Delta t=1/80$ in Fig. 9 are close to those with viscosity in Fig. 10. When the meshes are refined, less diffusion is introduced and the solution becomes closer to the solution with no viscosity. The scheme indeed catches the incompressible Euler limit and good numerical approximations can be obtained without resolving ϵ, which confirms the AP property that is proved in Section 4. However we need to take care of the numerical diffusion when coarse meshes are used. One possible way to improve this is to use less diffusive shock capturing schemes at first order or higher order schemes using the MUSCL strategy for instance [8,19,20], or to use staggered grid discretizations.

7 Conclusions

We propose an all speed scheme for the Isentropic Euler equations. The key idea is the semi-implicit time discretization, in which the low Mach number stiff pressure term is divided into two parts, one being treated explicitly and the other one implicitly. Moreover, the flux of the density equation is also treated implicitly. The parameter which tunes the explicit-implicit decomposition of the pressure term allows to suppress the nonphysical oscillations. We have provided a strategy for the choice of this parameter; this strategy depends on the time step and the fluid velocity. In future work, we will consider the possibility of making this parameter space-dependent, which will lead to an improved local fine-tuning of the scheme.

The numerical results show that the oscillations around shocks of $\mathcal{O}(\epsilon^2)$ strength can be suppressed by choosing α as in (5.15). The low Mach number limit of the time semi-discrete scheme becomes an elliptic equation for the pressure term, so that the density becomes a constant when $\epsilon \to 0$. In this way, the incompressible property is recovered in the limit $\epsilon \to 0$. Implemented with proper space discretizations, we can propose an AP scheme which can capture the incompressible limit without the need for Δt, Δx to resolve ϵ.

In this paper we demonstrate the potential of this idea by using the first order Rusanov scheme with local evaluation of the wave speeds. Though this first order method is quite dissipative, we can observe that the scheme is stable independently of ϵ and that the CFL condition is $\Delta t = \mathcal{O}(\Delta x)$ uniformly in ϵ. It can also capture the right incompressible limit without resolving the Mach number. Higher order space discretizations like the MUSCL method [8, 19, 20] can be built into this framework. This is the subject of current work.

This paper provides a framework for the design of a class of all speed schemes. Compared with the ICE method [12, 13] and some recent work by Jin et al. [11], the idea is simpler and more natural. This framework is a step towards the more physical case of the full Euler equations and flows with variable densities and temperatures. These extensions and applications [23] will be the subject of future work.

Acknowledgments

This work was supported by the French "Commissariat á l'Energie Atomique (CEA)" (Centre de Saclay) in the frame of the contract "ASTRE", # SAV 34 160 and by the Marie Curie Actions of the European Commission in the frame of the DEASE project (MEST-CT-2005-021122).

References

[1] H. Bijl and P. Wesseling, A unified method for computing incompressible and compressible flows in boundary-fitted coordinates, J. Comput. Phys., 141 (1998), 153–173.

[2] M. P. Bonner, Compressible Subsonic Flow on a Staggered Grid, master thesis, The University of British Columbia, 2007.
[3] P. Constantin, On the Euler equations of incompressible fluids, B. Am. Math. Soc., 44(4) (2007), 603–621.
[4] P. Crispel, P. Degond and M.-H. Vignal, An asymptotic preserving scheme for the two-fluid Euler-Poisson model in the quasineutral limit, J. Comput. Phys., 223 (2007), 208–234.
[5] P. Degond, F. Deluzet, A. Sangam and M-H. Vignal, An asymptotic preserving scheme for the Euler equations in a strong magnetic field, J. Comput. Phys., 228(10) (2009), 3540–3558.
[6] P. Degond, S. Jin and J.-G. Liu, Mach-number uniform asymptotic-preserving gauge schemes for compressible flows, B. I. Math., Academia Sinica, New Series, 2(4) (2007), 851–892.
[7] P. Degond, J.-G. Liu and M.-H. Vignal, Analysis of an asymptotic preserving scheme for the Euler-Poison system in the quasineutral limit, SIAM J. Numer. Anal., 46 (2008), 1298–1322.
[8] P. Degond, P. F. Peyrard, G. Russo and P. Villedieu, Polynomial upwind schemes for hyperbolic systems, Partial Differential Equations, 1 (1999), 479–483.
[9] F. Golse, S. Jin and C. D. Levermore, The convergence of numerical transfer schemes in diffusive regimes I: the discrete-ordinate method, SIAM J. Numer. Anal., 36 (1999), 1333–1369.
[10] J. R. Haack and C. D. Hauck, Oscillatory behavior of asymptotic-preserving splitting methods for a linear model of diffusive relaxation, Los Alamos Report LA-UR 08-0571, appeared in Kinetic and Related Models, 2008.
[11] J. Haack, S. Jin and J. G. Liu, All speed asymptotic preserving schemes for compressible flows, in preparation.
[12] F. H. Harlow and A. Amsden, A numerical fluid dynamics calculation method for all flow speeds, J. Comput. Phys., 8 (1971), 197–213.
[13] F. H. Harlow and J. E. Welch, Numerical calculation of time-dependent viscous incompressible flow of fluid with free surface, Phys. Fluid., 8(12) (1965), 2182–2189.
[14] R. I. Issa, A. D. Gosman and A. P. Watkins, The computation of compressible and incompressible flow of fluid with a free surface, Phys. Fluids., 8 (1965), 2182–2189.
[15] S. Klainerman and A. Majda, Singular limits of quasilinear hyperbolic systems with large parameters and the incompressible limit of compressible fluids, Commun. Pure. Appl. Math., 34 (1981), 481–524.
[16] S. Klainerman and A. Majda, Compressible and incompressible fluids, Commun. Pure. Appl. Math., 35 (1982), 629–653.
[17] R. Klein, Semi-implicit extension of a Godunov-type scheme based on low Mach number asymptotics I: one-dimensional flow, J. Comput. Phys., 121 (1995), 213–237.
[18] R. Klein, N. Botta, T. Schneider, C. D. Munz, S. Roller, A. Meister, L. Hoffmann and T. Sonar, Asymptotic adaptive methods for multi-scale problems in fluid mechanics, J. Eng. Math., 83 (2001), 261–343.
[19] A. Kurganov and E. Tadmor, New high-resolution central schemes for nonlinear conservation laws and convection-diffusion equations, J. Comput. Phys., 160 (2000), 214–282.
[20] A. Kurganov and E. Tadmor, Solution of two-dimensional Riemann problems for gas dynamics without Riemann problem solvers, Numer. Meth. Part. D. E., 18 (2002), 548–608.
[21] R. J. Leveque, Numerical Methods for Conservation Laws, Lectures in Mathematics ETH Zürich, 1992.
[22] R. J. Leveque, Finite Volume Method for Hyperbolic Problems, Cambridge Text in Applied Mathematics, Cambridge University Press, 2002.

[23] C. D. Munz, M. Dumbser and S. Roller, Linearized acoustic perturbation equations for low Mach number flow with variable density and temperature, J. Comput. Phys., 224 (2007), 352–364.
[24] C. D. Munz, S. Roller, R. Klein and K. J. Geratz, The extension of incompressible folw solvers to the weakly compressible regime, Comp. Fluid., 32 (2002), 173–196.
[25] J. H. Park and C. D. Munz, Multiple pressure variables methods for fluid flow at all Mach numbers, Int. J. Numer. Meth. Fluid., 49 (2005), 905–931.
[26] S. V. Patankar, Numerical Heat Transfer and Fluid Flow, New York: McGraw-Hill, 1980.
[27] F. Rieper and G. Bader, The influence of cell geometry on the accuracy of upwind schemes in the low Mach number regime, J. Comput. Phys., 228 (2009), 2918–2933.
[28] V. V. Rusanov, Calculation of interaction of non-steady shock waves with obstacles, J. Comput. Math. Phys., 1 (1961), 267–279.
[29] D. R. van der Heul, C. Vuik and P. Wesseling, A conservative pressure-correction method for flow at all speeds, Comput. Fluid., 32 (2003), 1113–1132.